Study on Thin Coaxial Antennas for Minimally Invasive Microwave Thermal Therapy

February 2001

Kazuaki SUMO

Graduate School of Science and Technology
Chiba University

（千葉大学学位申請論文）

Study on Thin Coaxial Antennas for Minimally Invasive Microwave Thermal Therapy

2001 年 2 月

千葉大学大学院自然科学研究科

人工システム科学専攻　電子・光システム講座

齊藤　一幸

Study on Thin Coaxial Antennas for Minimally Invasive Microwave Thermal Therapy
低侵襲マイクロ波温熱治療用微細径同軸構造アンテナの研究

Table of Contents

Chapter 1

Introduction

1.1 Minimally invasive microwave thermal therapy

In recent years, the QOL (Quality Of Life) of the patient becomes more important [1]. Therefore, it is recognized that medical applications of microwave are important. Because applications are effective for reduction of the mental and physical burden of the patients [2]. They can be classified as follows.

(1) Thermal treatments, which use the microwave energy as a heating source.

(2) Information gathering and diagnoses inside the human body, which use the microwaves, such as CT (Computer Tomography) and non-invasive temperature measurement inside the human body [3], [4].

(3) Picking up the medical information of the human body from the outside the body and information transmission [5].

In (2), diagnoses inside the human body using X-ray, ultrasound and magnetic field have been studied. However, in recent years, researchers have tried this by using the

microwave techniques. In (3), these techniques are considered to be an extension of communication technologies. Therefore, this dissertation describes the characteristics of the thin coaxial antennas for the minimally invasive microwave thermal therapies.

In recent few decades, various types of applications of the microwaves have been investigated and have been applied to thermal therapy. In particular, minimally invasive interstitial therapies using thin applicators have expanded dramatically. They are interstitial hyperthermia and microwave coagulation therapy for medical treatment of cancer, cardiac catheter ablation for ventricular arrhythmia treatment [6], [7], thermal treatment of BPH (Benign Prostatic Hypertrophy) [8], and so forth.

In particular, this dissertation focused on the antennas for the interstitial microwave hyperthermia and the microwave coagulation therapy both for thermal treatment of cancer. However, the results of this dissertation can be applied not only to hyperthermia and microwave coagulation therapy but also for improvement of the antennas for the cardiac catheter ablation, the treatment of BPH, and so forth. Because the antennas for that treatment and the antennas for the cancer treatment have some common characteristics (e. g. very thin diameter). Moreover, the results and discussions of this dissertation will give suggestions for not only the characteristics of the antenna inside the human body but also for the behavior of electromagnetic wave inside lossy media.

1.2 Hyperthermia

1.2.1 Brief explanation and biological basics

Hyperthermia is one of the modalities for cancer treatment, utilizing the difference of the thermosensitivity between the tumor and the normal tissue [9], [10]. Figure 1.1 shows the principle of hyperthermia. There is a difference of thermosensitivity of about 42-43 °C between them at the frontier. Therefore, if the tumor is heated to this temperature or more, the cancer cells can be selectively killed and damaged.

Surgical excitation, radiation therapy and chemotherapy are most common modalities for cancer therapy nowadays. However, they have a lot of constraints for the patient and side effects. In contrast with that, hyperthermia has less drawbacks. Moreover, it has the advantage to enhance the treatment effect further more, when coupled with radiation therapy and chemotherapy [9]. In addition, hyperthermia has been covered by the Health Insurance Plan in Japan since 1997 [10].

Biological backgrounds of hyperthermia lie in the phenomenon that the thermosensitivity of the tumor is higher than the one of the normal tissue [9], [10]. Reasons for such high thermosensitivity of the tumor are enumerated here after.

(1) Difference of cell cycle

There is only a slight difference of thermosensitivity between the cancer cells and the normal cells when they are not in proliferation period. However, the thermosensitivity increases during the cell-proliferation period. Thus, a normal cell will resist to

the heat better than a cancer cell, which has an infinite proliferation ability.

(2) Decrease of blood flow

In general, the blood flow in the tissue carries heat away. However, blood vessels in tumor are immature because they proliferate in a very short term. As a result, the blood flow in a tumor is lower than in a normal tissue. In addition, the blood flow in a tumor decreases above 43 °C, while the one in normal tissues increases. Therefore, rise of temperature in the tumor becomes higher than in normal tissues.

(3) State of low oxygen and low pH

The rate of oxygen in the tissue is in close relationship with the quantity of supplied blood flow. Consequently, the tumor is in a state of low oxygen by the lack of blood vessels. In general, low oxygen cells become less thermotolerable.

Moreover, when the pH of the cell is low, the thermosensitivity increases remarkably. The center of a large tumor is in state of low oxygen and low nourishment with low pH. These hypoxic and starved cells, which are often found in the tumor, are more highly thermosensitive than nourished cell. This state of low pH also improves the effect of killing and damaging the tumor.

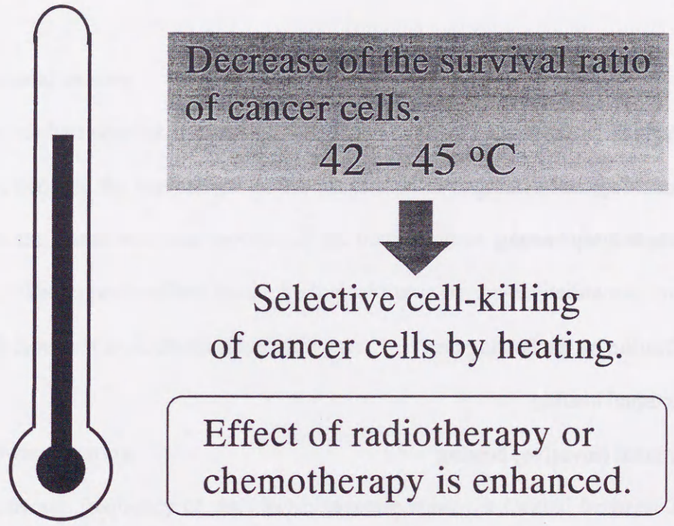

Fig. 1.1 Principle of the hyperthermia.

1.2.2 Classification of heating techniques

In the hyperthermia, there are several classification methods depending either on the heating region, the heating part and the heating energy. These methods are as follows [11].

(1) Classification by the heating region

Local/regional heating

Whole body heating

(2) Classification by the heating part

External heating

Internal (invasive) heating

(3) Classification by the heating energy

RF (Radio Frequency) heating

Ultrasound heating

Microwave heating

As this dissertation describes antennas for heating we will emphasize on the "heating energy". Therefore, the explanation of "heating energy" is described after.

(a) RF heating

RF is the abbreviation for Radio Frequency, and the method consist in by the mean

of electromagnetic waves with a frequency of several tens of MHz. There are capacitive heating and inductive heating when using this frequency band. In RF heating, deep-seated tumor can be treated. However, heat might be generated in the bones and the fat with high resistance.

(b) Ultrasound heating

This method consists in focusing the ultrasound in the tissue with plural oscillators. However, because the wavelength of the ultrasound in the biological tissue is short, air present in the bones and after cavities of the body-such as a bronchial tube-become an obstacle. The opposite effect on the biological tissue by the cavitation etc., may not be neglected though it is a non-invasive technique.

(c) Microwave heating

Microwave frequency of the electromagnetic waves is located between 300 MHz and 30 GHz. In hyperthermia, it is used approximately from 100 MHz to 3 GHz. Because attenuation is rapid at such a high frequency in the biological tissue, deep heating is difficult with the microwave heating. However, heating by the mean of microwaves achieves miniaturization of the equipment and improvement of the heating efficiency, and it makes treatment of the localized tumor possible.

1.2.3 Interstitial microwave hyperthermia

The interstitial microwave hyperthermia is used for treatment of large-volumed and deep-seated tumors. In the treatment, a thin microwave antenna is inserted into the tumor and the microwave energy heats up the tumor. The antenna usually employed is as an array applicator* allowing the insertion of several elements into the tissue as shown in Fig. 1.2. Such antennas can be utilized as an adjuvant therapy to the interstitial radiation therapy, by using the same catheter (This technique is presented in Section 4.5.).

In this figure, it is possible to change the heating pattern in the perpendicular direction of the antenna axis by varying the number of elements and the antenna insertion points. Concerning the control of the heating pattern in the longitudinal direction of the antenna axis is realized by changing the structure of the antenna elements [12], [13].

An example of interstitial heating system is shown in Fig. 1.3. The temperature in the tumor is monitored by the mean of inserted temperature sensors, and the output power of the microwave generator is modified by feedback control. The microwave power output from the generator feeds the antennas through a power divider.

* The term "applicator" indicates the part of the heating system, which is directly applied on the human body.

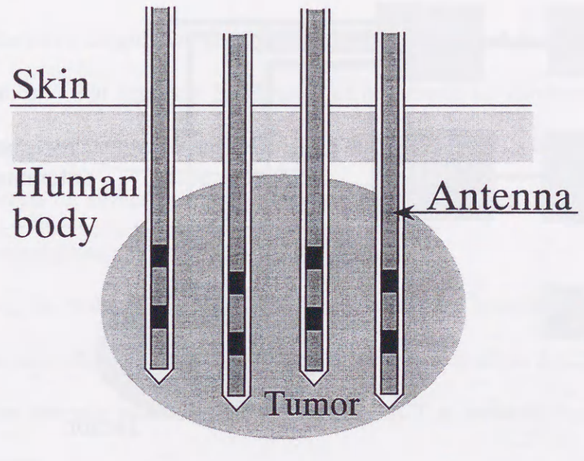

Fig. 1.2 Interstitial microwave hyperthermia.

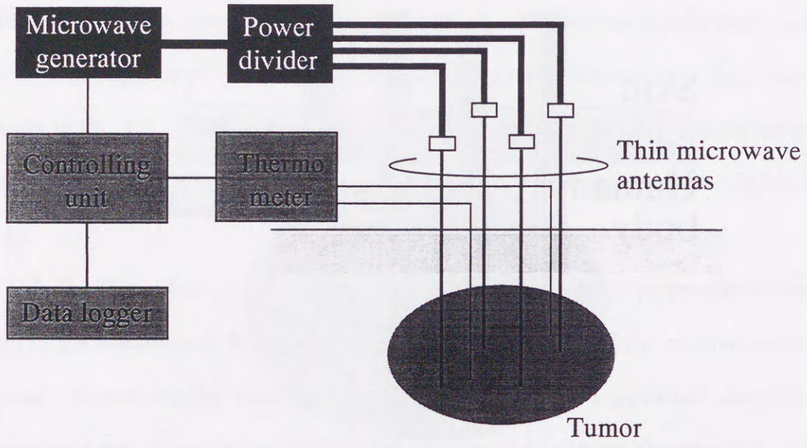

Fig. 1.3 Example of interstitial heating system.

1.3 Microwave coagulation therapy

1.3.1 Scheme of microwave coagulation therapy

The microwave coagulation therapy (MCT) has been used for the treatment of small size tumors. For instance: MCT used for hepatocellular carcinoma [14], [15]. In the treatment, the microwave energy heats up the target tissue (> 60 °C) to cause coagulation necrosis for several minutes or less (see Fig. 1.4). Therefore, MCT is useful to reduce the mental and physical burden of the patients.

Moreover, the biological basics of the hyperthermia are inducing a kind of apoptosis and cytotoxic effects of the cancer cells while the basics of the MCT are inducing the coagulation necrosis in the tumor. Therefore, MCT is powerful for treatment of small size tumors.

Figure 1.5 shows the basic configuration of the MCT under an ultrasonic guide. In this system, the input power of the antenna is of several tens of Watts. During the treatment, the doctor can observe the situation of the tissue coagulation inside the human body through the monitor of the ultrasonic guide.

In addition, there are some other types of MCT. For instance, MCT under observation laparoscope, combination of MCT and diagnosis by an endscope, and so on. However, in this dissertation, antennas for normal type of MCT (sometimes called percutaneous MCT (PMCT)) are described.

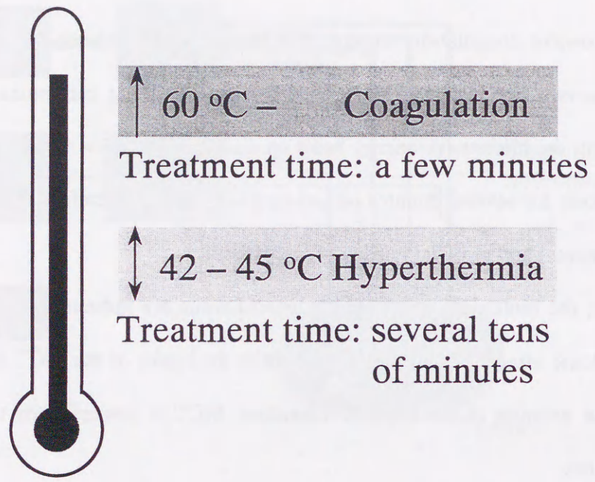

Fig. 1.4 Therapeutic temperature of the MCT.

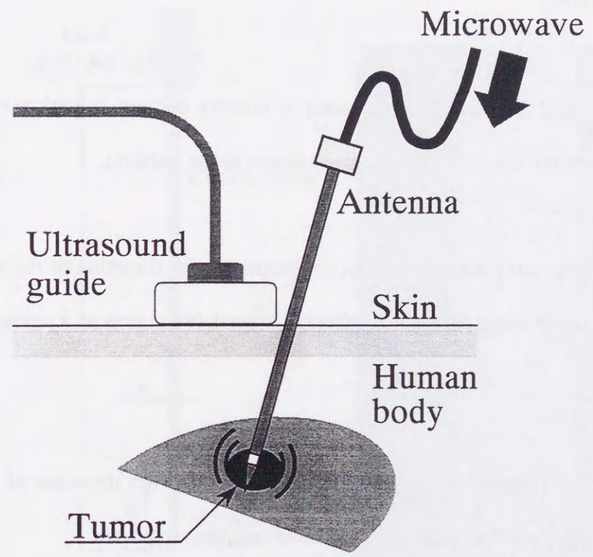

Fig. 1.5 Scheme of the MCT under an ultrasonic guide.

1.3.2 Problems with conventional antenna

Figure 1.6 shows the typical conventional antenna for MCT. This antenna is very effective for the treatment of small size tumors. However, some problems have to be improved as follows.

(1) In conventional antenna, the conductor is directly contact in with the coagulated tissues; therefore the coagulated tissue adheres to the antenna.

(2) The size of the coagulated region in the perpendicular direction of the antenna axis is insufficient in some cases. A spherical coagulated region of 3 cm in diameter is required.

(3) Length of the coagulated region becomes longer into the direction of the antenna insertion. Especially, spherical coagulated region is required.

In (1), to insert the antenna in a catheter prevents the adhesion of the coagulated tissues to the antenna. However, it is not so easy to solve other problems. In this dissertation, problem (2) will be overcome by introducing an array applicator composed of few antennas and problem (3) will be solved by introducing a new type of antenna.

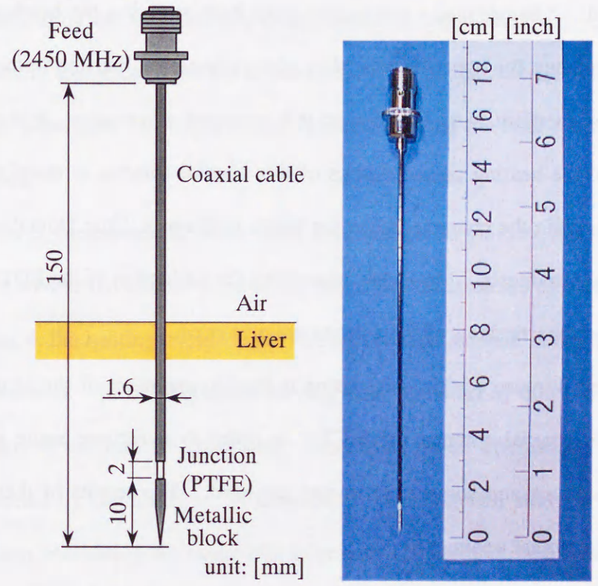

Fig. 1.6 Structure of the typical conventional MCT antenna.

1.4 Purpose of this study

There are two major purposes to this dissertation.

First, in the hyperthermic region, the heating characteristics of thin coaxial antenna are described. Though many researchers have been studying the heating characteristics of the antenna for hyperthermia, they always assumed that the human body is an homogeneous medium. As opposed to this common assumption, in this dissertation are described the heating characteristics of thin coaxial antenna in multilayered media. In order to explain the characteristics, the Finite Difference Time Domain (FDTD) calculations are introduced. Moreover, to confirm the validation of the FDTD calculation model, some characteristics of the antenna are measured.

Second purpose of this dissertation is the improvement of the heating performances of thin coaxial antenna for MCT. In order to overcome some problems, the FDTD calculations and some experiments are used. The results of these studies are very useful for actual treatments.

1.5 Contents

This dissertation deals with the heating characteristics of thin coaxial antennas for the minimally invasive microwave thermal therapies, particularly in the interstitial microwave hyperthermia and the microwave coagulation therapy (MCT).

In Chapter 2, analytical methods to obtain the heating characteristics of thin coaxial antenna are described. Analytical methods can be used for both the hyperthermic and MCT region.

In Chapter 3, measurement of the SAR distributions to validate the results of the calculations as well as the effectiveness of the improved antennas are presented.

In Chapter 4, the heating characteristics of thin coaxial antenna in the hyperthermic region are presented. In particular, the heating characteristics of thin coaxial antenna in the multilayered medium are described. Moreover, on-off controlled feeding technique is examined by calculation. In addition, the fundamental study to develop the treatment system combining the interstitial microwave hyperthermia and the interstitial radiation therapy is described.

In Chapter 5, the improvement of the coaxial antennas for the MCT is described. In this chapter, the antenna is improved in two ways. The first one is the construction of the array applicator by employing few antennas, and second is the introduction of a new type of antenna.

Finally conclusions of this dissertation are presented in Chapter 6.

References in Chapter 1

[1] K. Ito, "Medical applications of antenna techniques," Proceedings of 1998 Communications Society Conference of IEICE, vol. 1, TB-1-3, Sep.-Oct. 1998 (in Japanese).

[2] K. Ito, "Medical applications of microwave," Proceedings of 1996 Asia-Pacific Microwave Conference (New Delhi, India), vol. 1, pp. 257-260, Dec. 1996.

[3] S. Mizushina, H. Ohba, K. Abe, S. Mizoshiri, and T. Sugiura, "Recent trends in medical microwave radiometry," IEICE Transactions on Communications, vol. E-78B, no. 6, pp. 789-798, 1995.

[4] J. Montreuil and M. Nachman, "Multiangle method for temperature measurement of biological tissues by microwave radiometry," IEEE Transactions on Microwave Theory and Techniques, vol. 39, no. 7, pp. 1235-1238, 1991.

[5] K. Shimizu, S. Matsuda, I. Saito, K. Yamamoto, and T. Hatsuda, "Application of biotelemetry technique for advanced emergency radio system," IEICE Transactions on Communications, vol. E-78B, no. 6, pp. 818-825, 1995.

[6] H. M. Chiu, A. S. Mohan, D. Guy, S. P. Thomas, and D. L. Ross, "A novel array antenna based catheter for microwave cardiac ablation," Proceedings of the 2000 International Symposium on Antennas and Propagation (Fukuoka, Japan), vol. 1, pp. 233-236, Aug. 2000.

[7] R. D. Nevels, G. D. Arndt, G. W. Raffoul, J. R. Carl, and A. Pacifico, "Microwave catheter design," IEEE Transactions on Biomedical Engineering, vol. 45, no. 7, pp. 885-890, 1998.

[8] D. Despretz, J. C. Camart, C. Michel, J. J. Fabre, B. Prevost, J. P. Sozanski, and M. Chivé, "Microwave prostatic hyperthermia: interest of urethral and rectal applicators combination – Theoretical study and animal experimental results," IEEE Transactions on Microwave Theory and Techniques, vol. 44, no. 10, pp. 1762-1768, 1996.

[9] M. H. Seegenschmiedt, P. Fessenden, and C. C. Vernon (Eds.), "*Thermoradiotherapy and thermochemotherapy*," Springer-Verlag, Berlin, 1995.

[10] M. Hiraoka and Y. Tanaka (Eds.), "*Hyperthermia manual, revised edition*," Iryo-kagakusha, Tokyo, 1999 (in Japanese).

[11] L. Hamada, "Study on the array applicator for microwave interstitial hyperthermia," Ph. D. dissertation at Chiba University, Chiba Japan, Feb. 2000.

[12] L. Hamada, K. Saito, H. Yoshimura, and K. Ito, "Dielectric-loaded coaxial-slot antenna for interstitial microwave hyperthermia: longitudinal control of heating patterns," International Journal of Hyperthermia, vol. 16, no. 3, pp. 219-229, 2000.

[13] K. Saito, L. Hamada, H. Yoshimura, and K. Ito, "Control of heating pattern to the insertion direction in array applicator for interstitial microwave hyperthermia," Japanese Journal of Hyperthermic Oncology, vol. 15 (suppl.), pp. 304-305, Sep. 1999 (in Japanese).

[14] T. Seki, M. Wakabayashi, T. Nakagawa, T. Itoh, T. Shiro, K. Kunieda, M. Sato, S. Uchiyama, and K. Inoue, "Ultrasonically guided percutaneous microwave coagulation therapy for small carcinoma," Cancer, vol. 74, no. 3, pp. 817-825, 1994.

[15] R. Murakami, S. Yoshimatsu, Y. Yamashita, T. Matsukawa, M. Takahashi, and K. Sagara, "Treatment of hepatocellular carcinoma: value of percutaneous microwave coagulation," American Journal of Roentgenology, vol. 164, pp. 1159-1164, May 1995.

Chapter 2

Coaxial-slot antenna and calculation methods

2.1 Introduction

This chapter describes the structure of the coaxial-slot antenna, as well as the numerical techniques for the heating characteristics of the thin coaxial antennas. The coaxial-slot antenna is one of the thin coaxial antennas used for the interstitial heating. Some researchers have been studying the coaxial-slot antenna [1]-[3]. In this dissertation, the coaxial-slot antenna is used for both the hyperthermia and the MCT.

In this chapter, the basic structure of the coaxial-slot antenna is explained at the beginning. In addition, SAR (Specific Absorption Rate), which is one of the important heating characteristics of the antenna for interstitial heating, is explained.

Moreover, the calculation model of the electromagnetic analysis by the Finite Difference Time Domain (FDTD) method is described. Finally, the numerical technique of the temperature simulation in the human body is presented.

2.2 Coaxial-slot antenna

The coaxial-slot antenna is one of the applicators used for the interstitial heating. The basic structure of the coaxial-slot antenna is shown in Fig. 2.1. This antenna is composed of a thin semirigid coaxial cable, whose outer diameter is approximately 1.0 mm. The tip of the cable is short-circuited and several number of ring slots are cut on the outer conductor. The heating pattern around the antenna can be modified by changing the structure of the slots such as position and width. The antenna is designed to be embedded into a catheter for medical safety, therefore this applicator can be applied as adjuvant therapy to interstitial radiation therapy, by using the same catheter.

The structural parameters of the antenna are defined as follows (see Fig. 2.1):

d_b : the outer diameter of the antenna cable,

d_c : the outer diameter of the catheter,

D_t : the insertion depth,

L_{ls} : the length from tip to the nearest slot from the tip,

L_{ts} : the length from the tip to the nearest slot from the feed,

N_{sl} : the number of the slots,

t_c : the thickness of the catheter,

W_{sl} : the width of the slot (in this study, W_{sl} is set to 1.0 mm),

ε_{rc} : the relative permittivity of the catheter,

ε_{ri} : the relative permittivity of the inner dielectric.

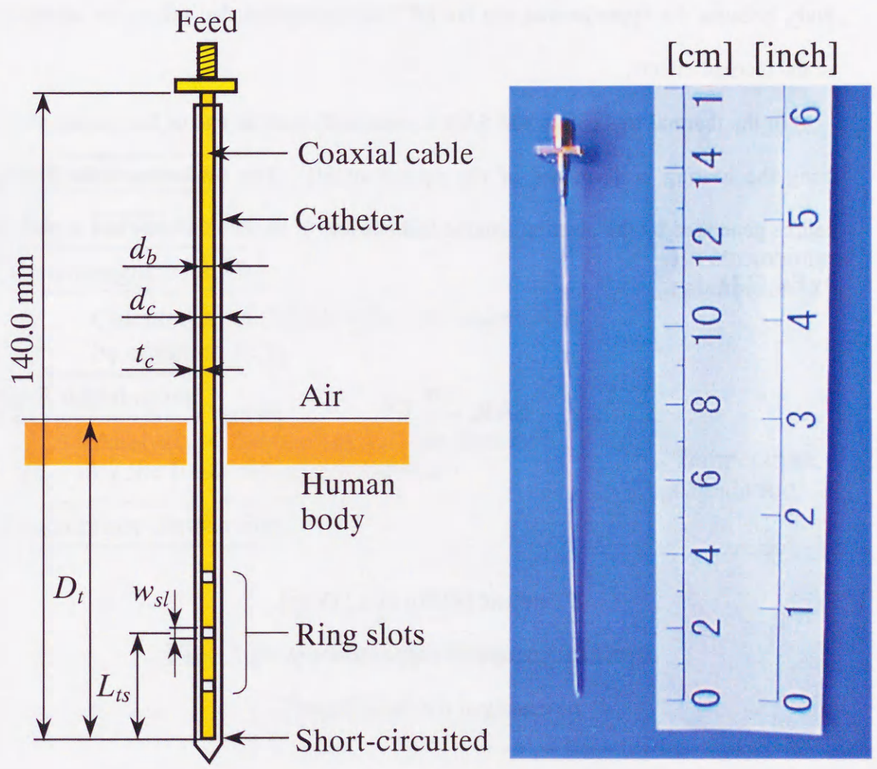

Fig. 2.1 Basic structure of the coaxial-slot antenna.

2.3 Procedure for analysis

The goal of the calculation is to obtain the temperature distribution in the human body, because the hyperthermia and the MCT are treatments that utilize the advantage of the thermal effects.

In the thermal treatments, the SAR is commonly used as one of the indices evaluating the heating performance of the equipment [4]. The SAR shows the heating source generated by the electromagnetic fields inside of the human body and is defined by Eq. (2.1).

$$\mathrm{SAR} = \frac{\sigma}{\rho} E^2 \qquad [\mathrm{W/kg}] \qquad (2.1)$$

where,

E : electric field (r. m. s.) [V/m],

σ : conductivity of the tissue [S/m],

ρ : density of the tissue [kg/m^3].

The procedure of the calculation is shown in Fig. 2.2. At first, the SAR distribution around the antenna is calculated. After the SARs are obtained, the temperature distribution is calculated from the SAR by numerical analysis (Finite Difference Method: FDM) of the bioheat transfer equation [5]. In this calculation, the same grid as those of the electromagnetic calculation and only calculated inside the tissue.

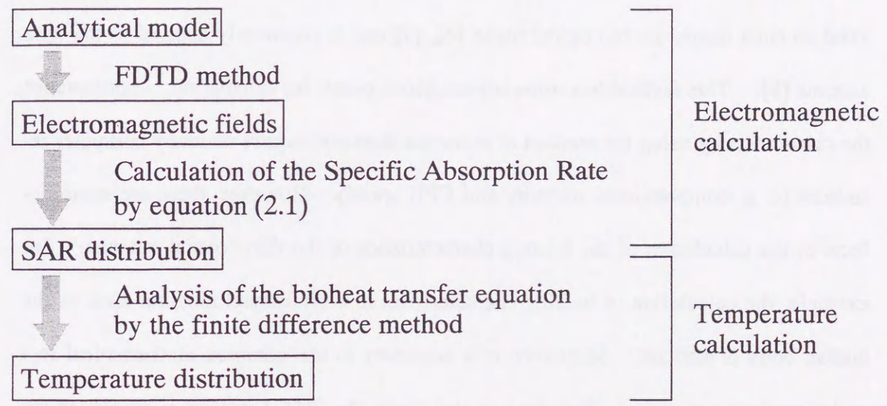

Fig. 2.2 Procedure of the calculation.

2.4 FDTD calculation model

The FDTD method is one of the numerical techniques, which solves the Maxwell's equations of differential form in the time domain (The brief explanation of the finite difference approximations are showed in Appendix 1). However, the method of moments has been used for the estimation of the electromagnetic field around the thin coaxial antenna inside the biological tissue [6], [7] and is commonly applied to the wire antenna [8]. This method has some advantageous points for calculation. For instance, the calculation by using the method of moments does not require so many computer resources (e. g. computational memory and CPU speed). However, there are some defects in the calculation of the heating characteristics of the thin coaxial antenna. For example, the calculation of heating characteristics in a multilayed medium such as the human body is difficult. Moreover, it is necessary to use complex mathematical formulations in some cases. Therefore, in this study, the FDTD method is employed for the calculation of the electromagnetic field around the antenna [9], [10]. Because, in general, though the FDTD calculation requires a large number of computational memories and high speed CPU, this method has high generality especially in the complex structure.

Figure 2.3 shows the typical FDTD calculation model [11], [12]. For modeling the coaxial-slot antenna precisely, a very fine mesh model, which wastes large computational memory and is time consuming, is needed because the antenna is very thin. Therefore, in this dissertation, a rectangular cross section is employed instead of a transverse cross section of the antenna. The validation of this calculation model will

be described in Chapter 4 and 5. A steady state analysis was performed, enforcing a sinusoidal electric field between the inner and the outer conductors of the coaxial cable. The outer boundary condition of the FDTD space was the Mur first order [10]. Moreover, the human body including the target tumor was modeled as a homogeneous medium for simplicity, which had the same physical characteristics as normal tissue (e. g. muscle or liver).

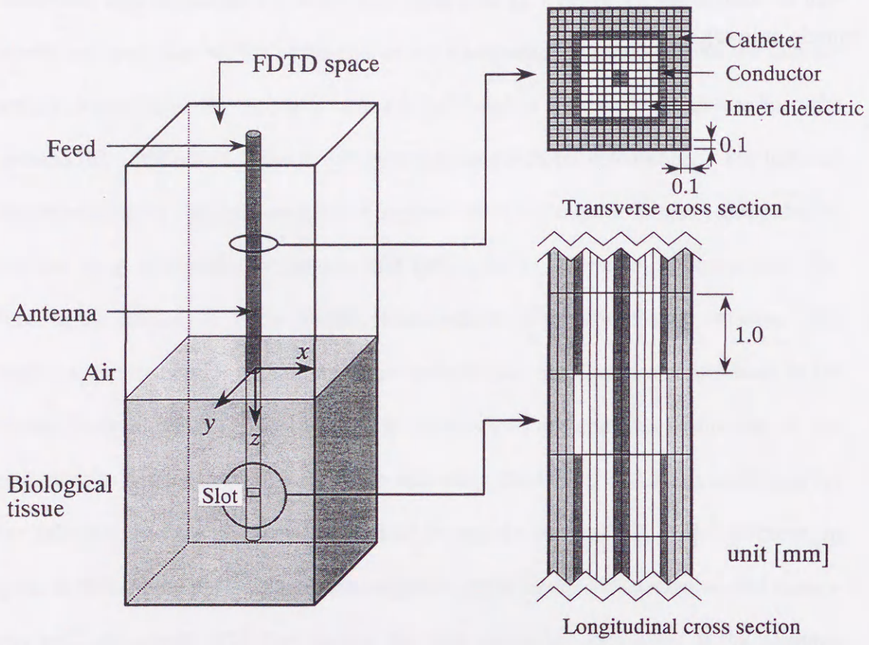

Fig. 2.3 FDTD calculation model for the coaxial-slot antenna.

2.5 Temperature calculation

The temperature distribution inside the human body is calculated by the FDM. As for the temperature distribution, various thermal models have been proposed, however, their validity still have not been clarified experimentally. Therefore, in this dissertation, the Pennes' bioheat transfer equation [5] was employed because it is the most practical engineering approximation at present.

The FDM can be classified into two types. These are the implicit method and the explicit method [13]. In the implicit method, though it is necessary to solve a large-scale simultaneous liner equation, we are able to choose arbitrarily the time step for the calculation. On the other hand, in the explicit method, though it is simple for mathematical formulation, the time step of calculation has to satisfy the stability criterion. In this dissertation, the implicit method is employed as the analysis of the antenna for the hyperthermia, and the explicit method is used for the analysis of the antenna for the MCT. Because in the analysis of the heating characteristics of the antenna for the MCT, to consider the effect of temperature-dependent electrical properties of the tissue, the explicit method was employed for simple calculation.

The bioheat transfer equation is given as by:

$$\rho\, c \frac{\partial T}{\partial t} = \kappa \nabla^2 T - \rho\, \rho_b\, c_b\, F \left(T - T_b\right) + \rho \cdot \mathrm{SAR} \qquad (2.2)$$

where,

T : temperature [°C],
t : time [s],
ρ : density [kg/m^3],
c : specific heat [J/kg·K],
κ : thermal conductivity [W/m·K],
ρ_b : density of the blood [kg/m^3],
c_b : specific heat of the blood [J/kg·K],
T_b : temperature of the blood [°C],
F : blood flow rate [m^3/kg·s].

The first, second and third terms in the right side of Eq. (2.2) denote the thermal conduction, the heat dissipation by the blood flow and the heat generation by the electric field, respectively. In this dissertation, we assumed that the temperature of the blood T_b is equal to the initial temperature of the tissue. The blood flow rate is the volume of blood that passes through a unit of mass of tissue per unit of time.

The finite difference approximation (explicit method) is shown in Appendix 2.

2.6 Conclusions in this chapter

This chapter has described the basic structure of the coaxial-slot antenna and the numerical techniques for the electromagnetic calculation, and the bioheat transfer equation for the analysis of temperature distribution in the human body. The basic structure of the coaxial-slot antenna has been explained at the beginning, then the SAR has been explained, and the calculation model of the coaxial-slot antenna by the FDTD method has explained. Finally, two numerical techniques for the temperature calculation (the implicit method and the explicit method) have been briefly described.

References in Chapter 2

[1] K. Ito, K. Ueno, M. Hyodo, and H. Kasai, "Interstitial applicator composed of coaxial ring slots for microwave hyperthermia," Proceedings of the 1989 International Symposium on Antennas and Propagation (Tokyo, Japan), vol. 2, pp. 253-256, Aug. 1989.

[2] M. Leoncini and G. B. Gentili, "EM modelling of microwave hyperthermic applicators by using the finite-difference time-domain (FDTD) method," Proceedings of the 1996 International Symposium on Antennas and Propagation (Chiba, Japan), vol. 4, pp. 1261-1264, Sep. 1996.

[3] H. M. Chiu, A. S. Mohan, D. Guy, S. P. Thomas, and D. L. Ross, "A novel array antenna based catheter for microwave cardiac ablation," Proceedings of the 2000 International Symposium on Antennas and Propagation (Fukuoka, Japan), vol. 1, pp. 233-236, Aug. 2000.

[4] M. H. Seegenschmiedt, P. Fessenden, and C. C. Vernon (Eds.), "*Thermoradiotherapy and thermochemotherapy*," Springer-Verlag, Berlin, 1995.

[5] H. H. Pennes, "Analysis of tissue and arterial blood temperatures in the resting human forearm," Journal Applied Physiology, vol. 1, pp. 93-122, 1948.

[6] M. S. Wu, "Study on the coaxial-slot antenna for interstitial microwave hyperthermia," Ph. D. dissertation at Chiba University, Chiba, Japan, Jul. 1995 (in Japanese).

[7] L. Hamada, M. S. Wu, K. Ito, and H. Kasai, "Basic analysis on SAR distribution of coaxial-slot antenna array for interstitial microwave hyperthermia," IEICE Transactions on Electronics, vol. E-78C, no. 11, pp. 1624-1631, 1995.

[8] W. L. Stutsman and G. A. Thiele, "*Antenna theory and design*," John Wiley & Sons, New York, 1981.

[9] K. S. Yee, "Numerical solution of initial boundary value problems involving Maxwell's equations in isotropic media," IEEE Transactions on Antennas and Propagations, vol. AP-14, no. 3, pp. 302-307, 1966.

[10] T. Uno, "*Finite difference time domain method for electromagnetic field and antenna analyses*," Corona publishing, Tokyo, 1998 (in Japanese).

[11] K. Saito and K. Ito, "Study on SAR distribution of coaxial-slot antenna for interstitial microwave hyperthermia using FDTD method," Transactions of the IEICE, vol. J82-B, no. 2, 276-282, 1999 (in Japanese).

[12] K. Saito, O. Nakayama, L. Hamada, H. Yoshimura, and K. Ito, "Basic study of the coaxial-slot antennas for minimally invasive microwave thermal therapy," Proceedings of the 20th Annual International Conference of the IEEE Engineering in Medicine and Biology Society (Hong Kong, China), vol. 20, pp. 3261-3264, Oct-Nov. 1998.

[13] G. D. Smith, "*Numerical solution of partial differential equations*," Science-sha, Tokyo, 1971.

Chapter 3

Measurement of the SAR distributions

3.1 Introduction

As mentioned earlier, the SAR distributions around the antenna are one of the most important indices for evaluating the heating performances of the antenna. The SAR distributions around the antenna can be obtained by numerical calculation. However, measurement of the SAR distributions is very important in the following situations.

(1) It is necessary to measure the SAR distributions when the calculation is impossible. For instance, the calculation of the SAR is impossible for the devices with complex structure, such as actual cellular phone placed near the human head [1]. Because construction of the precise calculation model of the actual cellular phone is impossible.

(2) Validation of the calculated results.

(3) Final checking of the heating performances of the heating devices.

In this dissertation, the SAR distribution is measured for the reason (2). This

chapter describes two different methods: the thermoghraphic method [1], [2] and the E-field method [3]. The validations of the numerical calculations by using these methods are described in Chapters 4 and 5.

3.2 Thermographic method

Figure 3.1 shows the scheme of the thermographic method by using an infrared camera and a tissue-equivalent solid phantom. First, the phantom is exposed to the microwaves radiated from the antenna. Then, the temperature-rise on the arbitrary cross section of the phantom is observed by using the infrared camera, after splitting the phantom. To minimize the heat diffusion in the phantom, the time of exposure time must be as short as possible within a range that makes the heat distribution observable.

If the heat diffusion and the exposure time are negligibly small, the SAR is given by Eq. (3.1),

$$\mathrm{SAR} = c\,\frac{\Delta T}{\Delta t} \qquad [\mathrm{W/kg}] \qquad (3.1)$$

where,

c : specific heat of the phantom [J/kg·K],

ΔT : temperature rise [K],

Δt : heating time [s].

The tissue-equivalent solid phantom developed in our laboratory is used. This phantom has almost the same electrical constant as the one of biological tissue (brain, muscle, skull, etc.) in microwave frequency. The phantom is made of deionized water, polyethylene powder, agar, TX-151 (Oil Center Research Inc. LA. USA), sodium chloride,

and preservatives (dehydroacetic acid sodium salt). In this dissertation, the muscle-equivalent phantom is used to study the heating characteristics of the antenna for the hyperthermia, and the liver-equivalent phantom is employed for the improvement of the antenna for the MCT. Tables 3.1 and 3.2 show the ingredients of the muscle and the liver-equivalent phantom, respectively.

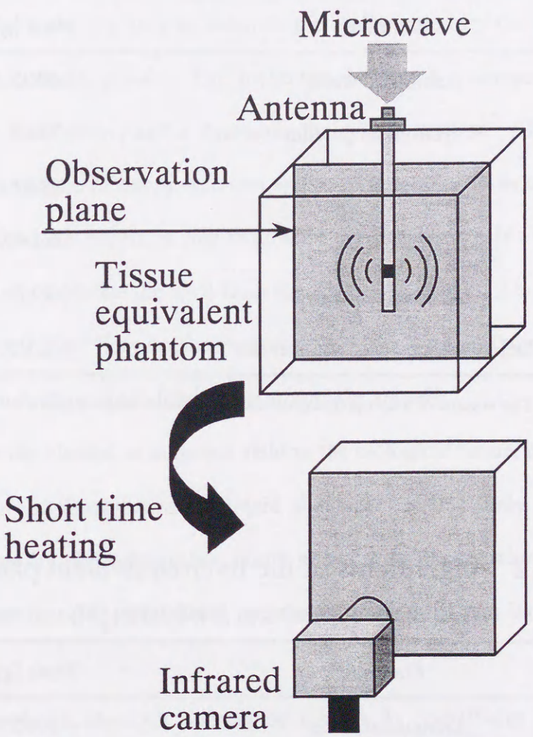

Fig. 3.1 Thermographic method.

Table 3.1 Ingredients of the muscle-equivalent phantom.

(ε_r = 53.0, σ = 1.41 S/m (430 MHz) [4])

Material	Mass [g]
Deionized water	3375
Polyethylene powder	337.5
Agar	104.6
TX-151	84.4
Sodium chloride	39.2
Dehydroacetic acid sodium salt	2.0

The volume of a completed phantom is approximately 3500 cm^3.

Table 3.2 Ingredients of the liver-equivalent phantom.

(ε_r = 43.03, σ = 1.69 S/m (2450 MHz) [5])

Material	Mass [g]
Deionized water	3375
Polyethylene powder	668.5
Agar	104.6
TX-151	46.1
Sodium chloride	28.2
Dehydroacetic acid sodium salt	2.0

The volume of a completed phantom is approximately 4000 cm^3.

3.3 E-field method

Figure 3.2 shows a picture of the SAR measurement system by the E-field method [3]. This system is widely used to estimate the SAR caused by the electromagnetic radiation from the cellular phone. This measurement system is composed of a robotic arm, an electric field probe, and a computer for system control. The electric field probe is placed at the tip of the robotic arm and is composed of three electrically short dipoles. Therefore, the system is able to directly measure the electric field around the antenna and directly calculate the SAR from Eq. (2.1). Moreover, it is able to measure not only the electric field but also the magnetic field by changing the probe. So, it is also able to measure the current distribution around the antenna.

To measure the electric or magnetic field in the biological tissue, it is necessary to scan the probe in the tissue-equivalent liquid phantom. In this study, this situation is realized by filling the tissue-equivalent liquid phantom in the container shown in Fig. 3.3. In this container, the coaxial-slot antenna is inserted 70 mm into the biological tissue.

In this dissertation, the SAR distribution around the coaxial-slot antenna and the current distribution on the antenna are measured by using that system.

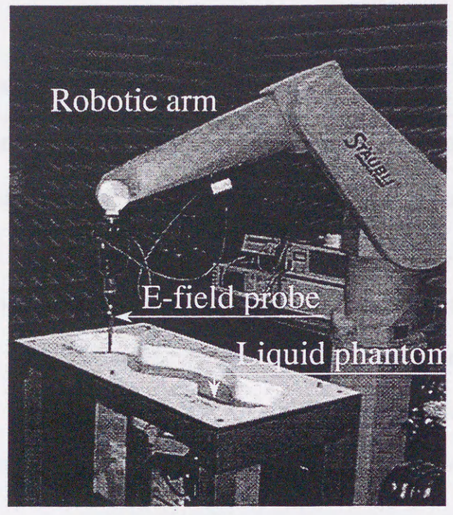

Fig. 3.2 Measurement system by the E-field method.

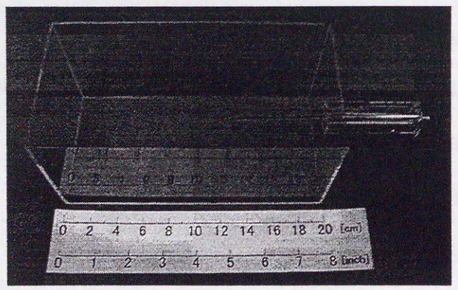

Fig. 3.3 Container for measurement of the E-field.

3.4 Conclusions in this chapter

This chapter has described two measurement methods of the SAR distributions: the thermographic method and the E-field method.

The thermographic method consistes in the measurement of the temperature distribution on the surface of the solid phantom. Therefore, the characteristics and the ingredients of the solid phantom have also been described. Refer to [6] for more detailed information on the thermographic method.

The E-field method is widely used to estimate the SAR caused by the electromagnetic radiation from the cellular phone. In this chapter, a brief explanation to use the measurement system for estimation of the SAR distributions around the interstitial antenna was described.

The measurement results by using these methods are shown in Chapters 4 and 5.

References in Chapter 3

[1] Y. Okano, A. Hase, I. Ida, and K. Ito, "A study on the estimation of SAR in human head for electromagnetic energy exposure," 1998 Asia-Pacific Microwave Conference Proceedings (Yokohama, Japan), vol. 3, pp. 1287-1290, Dec. 1998.

[2] K. Ito, L. Hamada, T. Asahina, and H. Yoshimura, "Phantoms for estimation of interaction between antennas and human body," Abstracts of Millenium Conference on Antennas & Propagation (Davos, Switzerland), vol. 1, Apr. 2000.

[3] T. Schmid, O. Egger, and N. Kuster, "Automated E-field scanning system for dosimetric assessments," IEEE Transactions on Microwave Theory and Techniques, vol. 44, no. 1, pp. 105-113, 1996.

[4] C. C. Johnson and A. W. Guy, "Nonionizing electromagnetic wave effects in biological materials and systems," Proceedings of IEEE, vol. 60, no. 6, pp. 692-719, 1972.

[5] http://www.fcc.gov/fcc-bin/dielec.sh

[6] Y. Okano, "The study on the evaluation of the mutual interaction between the high-frequency near-fields and the human body," Ph. D. dissertation at Chiba University, Chiba, Japan, Jan. 1999 (in Japanese).

Chapter 4

Heating characteristics of thin coaxial antennas in the hyperthermic region

4.1 Introduction

This chapter describes the heating characteristics of the coaxial-slot antennas for the interstitial microwave hyperthermia. First, in Section 4.2, the validity of the calculation model is confirmed by considering the SAR distribution around the antenna and the current distribution on the antenna. After the validation, the heating characteristics of the coaxial-slot antenna in the multilayered medium are described [1]. Second, in Section 4.3, the validity of the temperature calculation model is confirmed and the temperature distributions in the multilayered medium of the four-antenna array applicator are explained. In addition, an improvement of the temperature distributions in the multilayered medium by introducing the on-off feeding is presented [2]. Third, in Section 4.4, the possibility of heating patterns-control of the array applicator in the antenna insertion direction is considered [3]. Finally, in Section 4.5, the fundamental study for developing the treatment system combining the interstitial microwave hyperthermia and the interstitial radiation therapy is explained.

In this chapter, the feeding frequencies are assumed to be 430 and 2450 MHz.

The frequencies belong to the ISM (Industrial, Scientific, and Medical) frequencies [4], and are often used for thermal treatment in Japan. 430 MHz is good for a large-volumed heating and 2450 MHz is suitable for the localized heating inside the human body.

4.2 SAR distributions of single antennas

4.2.1 Validation of calculation model

In this section, the validity of the calculation model is confirmed. In this dissertation, the rectangular cross section model employed as the transverse cross section of the coaxial-slot antenna. So, the validity of this calculation model is described by the following procedure.

(1) SAR distribution near the antenna.

(2) Calculation of the characteristic impedance of the coaxial line.

(3) Comparison between the calculated and the measured SAR distributions in the direction of the antenna axis (by employing the E-field method).

(4) Calculated and measured current distribution on the antenna.

(1) SAR distribution near the antenna

Here, two types of shape for the cross section as shown in Fig. 4.1 are employed for the coaxial-slot antenna. In Fig. 4.2, the calculation results of the SAR distributions near the antenna are plotted by means of the FDTD calculation model for both the A and B (only quarter region is shown due to structural symmetry in the *x*-*y* plane). The parameters for calculation are shown in Table 4.1. Moreover, for the computation, a workstation and a Hitachi super computer S-3800 at Chiba University Information Processing Center are used.

Table 4.1 Parameters for calculations.

FDTD parameters	
Size of FDTD space	$x \times y \times z = 20 \times 20 \times 160$ mm
Cell size	$\Delta x = \Delta y = 0.1$ mm, $\Delta z = 1.0$ mm
Time step Δt	0.235 ps (from Courant limit)
Antenna structure	
Feeding frequency	430 MHz
L_{ts}	20.0 mm
D_t	70.0 mm
d_b	1.19 mm
d_c	2.00 mm
t_c	0.35 mm
ε_{rc}	3.50
ε_{ri}	2.03
Biological tissue	
Muscle [5]	$\varepsilon_r = 53.0$, $\sigma = 1.41$ S/m, $\rho = 1000$ kg/m^3

In the model with a rectangular cross section, if the corner portion affects the surrounding SAR distributions significantly, the problem is serious. However, it is found from this figure that, although an effect of the edge portions exists, this effect is negligible at locations away of about 1 mm from the surface of the antenna (catheter) so that the SAR distributions are not very different from those of staircasing approximation model. Therefore, in calculation of the SAR distributions, which is the most important

characteristics of the hyperthermic antenna, the effects of the edges are considered small in the rectangular cross section model in the model B.

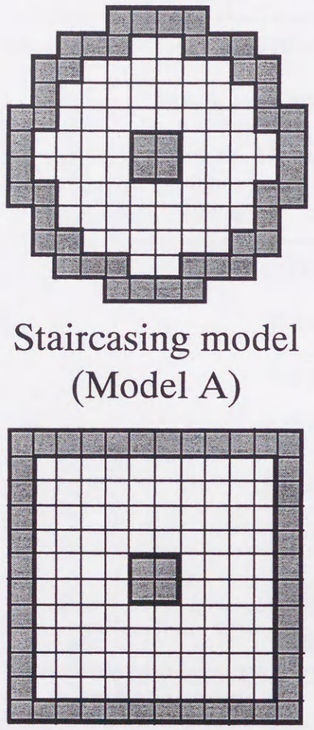

Staircasing model
(Model A)

Rectangular model
(Model B)

Fig. 4.1 Cross sections of the calculation model.

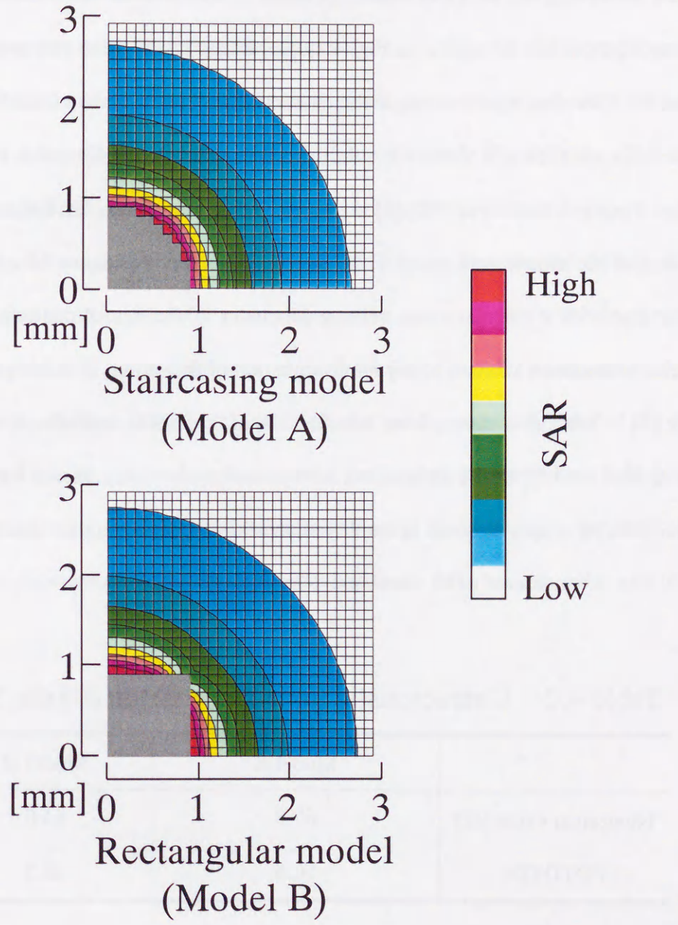

Fig. 4.2 The SAR distributions on the corner.

(2) Characteristic impedance of the coaxial line

By observing the characteristic impedance of the coaxial line with two types of cross section models as shown in Fig. 4.1, characteristics of these two models are understood. The numerical values of the characteristic impedance and the FDTD calculated results are shown in Table 4.2. In this FDTD calculation, Gaussian pulse feeding and fast Fourier transform (FFT) [6] are employed as a feeding. In Table 4.2, numerical value of the model A is meant to be the characteristic impedance of a conventional coaxial line with a circular cross section (diameter of the center conductor: 0.2 mm, diameter of the inner dielectric: 1.0 mm) while that of the model B is derived from Reference [7]. From this comparison, it is found that the FDTD result for the rectangular cross section model (model B) is closer to the numerical value. If a cell which size is smaller than $\Delta x = \Delta y = 0.1$ mm is employed and the staircasing approximation used, the coaxial line is considered to be simulated more accurately.

Table 4.2 Characteristic impedance of the coaxial line.

	Model A	Model B
Numerical value [Ω]	67.8	64.0
FDTD [Ω]	50.6	60.2

From above, we see that the rectangular cross section model can provide sufficient accuracy in the present analysis. Therefore, in this dissertation, various studies are conducted with this model.

(3) Calculated and measured SAR distributions in the direction of the antenna axis

Figure 4.3 shows the measured and the calculated SAR distributions in the direction of the antenna axis. The E-field method shown in Fig. 4.3 (a) is employed for SAR measurement. Here, the net input power (input power minus reflection power) of the antenna is 1 W, and the SAR observation line is shown in Fig 4.3 (b). The structure of the antenna and parameters for calculation are shown in Table 4.1.

From Fig. 4.3 (a), a difference of less than 30 % exists between the calculated and the experimental result in the SAR peak value. The reason of this result is caused by the positioning error of the E-field probe, indeed the probe is thick compared to the diameter of the coaxial-slot antenna. In addition, the small positioning error of the probe causes the SAR measurement error, because the inclination of the electric field is large near the antenna. From above, the calculation model is appropriate for analysis in terms of SAR distributions in the direction of the antenna axis.

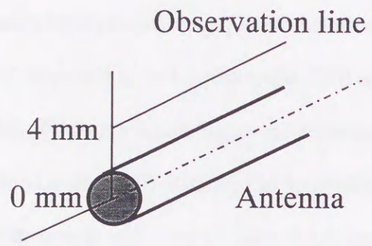

(a) Observation line.

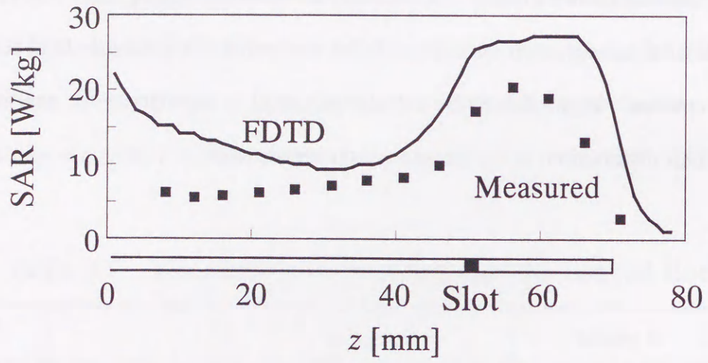

(b) SAR distributions on the observation line.

Fig. 4.3 SAR distributions in the direction of the antenna axis.

(4) Calculated and measured current distribution

Figure 4.4 shows comparison between the measured and the calculated current distribution on the coaxial-slot antenna. Here, the structure of the antenna and parameters for calculation are shown in Table 4.1. Both results are normalized to the maximum amplitude. In the FDTD calculation, the current distribution is defined as the strength of the magnetic field in the orthogonal direction to the antenna axis. Also, for the measurement of the current distribution, the strength of the magnetic field near the antenna is measured by using the measurement system shown in Fig. 3.2 with infinitesimal loop probe [8]. Although the tendencies are similar between the calculated and measured result, there is a slightly difference from the position of the slot to the antenna insertion point. It is due to the effect of the container filled with the liquid phantom used in this measurement. Therefore, we can say that the calculation model is useful for estimating the characteristics of the coaxial-slot antenna.

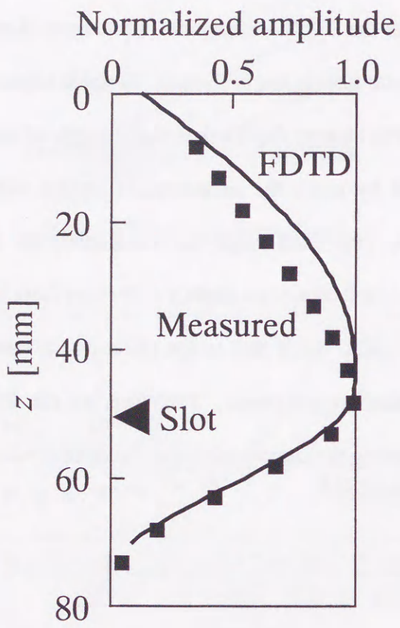

Fig. 4.4 Current distributions on the antenna.

4.2.2 Evaluation of hot spot

In the interstitial heating technique, control of the heating patterns in the longitudinal direction of implanted applicators has been regarded as important [9]. Particularly, it is very important for the applications to realize heating at the tip and to suppress the hot spots near the surface of the human body.

If the tip heating cannot be satisfied, the tumor would be penetrated by the antenna during the treatment and the normal tissues underlying the tumor could be damaged. Moreover, when the hot spots appear in the vicinity of the antenna insertion point, the patient feels fever there and the accomplishment of treatment can even become difficult because of the pain in the worst case.

The tip heating can be almost realized by making slots near the tip of the antenna. But, it is not so easy to suppress the hot spots when the insertion depth of the antenna is small. However, accurate estimation of the SAR value at the surface of the human body is impossible with the method of moment using the complex image method previously employed before [10], [11]. In this method, the error near the medium boundary becomes large so that accurate SAR values in such region cannot be obtained. Also, it is difficult to measure precisely the values by the thermographic method. Therefore, in this section, the SAR value of the surface of the human body are described by using the FDTD method.

Figure 4.5 (b) shows the calculated SAR distributions by the FDTD method on the observation line shown in Fig. 4.5 (a) that is the parallel line to the antenna axis located at 2 mm from the center of the antenna. The calculated result by the method of moment is shown in Fig. 4.5 (c) for comparison. In the result of the method of moment,

the value of the SAR at the medium surface is computed to be 1.5 times the SAR at the tip of the antenna. On the other hand, when the FDTD method is used for the calculation, the value of this portion is found to be approximately 85 % of the peak SAR.

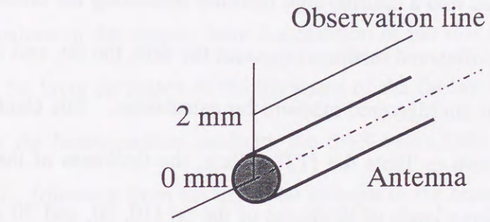

(a) Observation line.

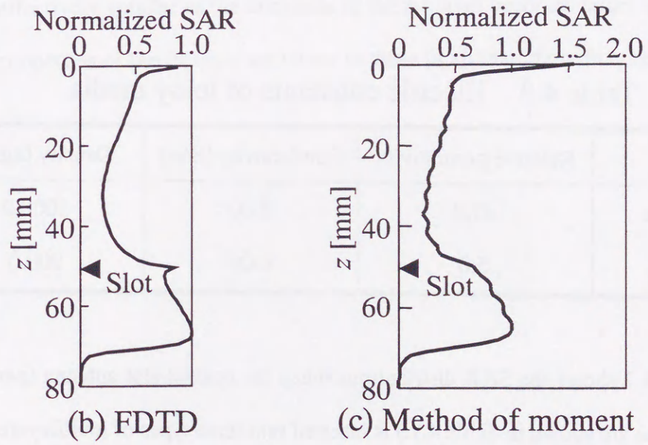

(b) FDTD (c) Method of moment

Fig. 4.5 SAR distributions around the coaxial-slot antenna.

4.2.3 SAR distributions in a multilayered medium

In this section, the SAR distributions around the antenna are calculated when the coaxial-slot antenna is inserted into a multilayered medium simulating the cross section of the human body. The multilayered medium represent the skin, the fat, and the muscle. Figure 4.6 illustrates the multilayered medium for calculation. The electric constants of these media are shown in Table 4.3 [12]. Here, the thickness of the skin is fixed to 2 mm. However, three kinds of thickness of the fat (10, 20, and 30 mm) are calculated for considering the individual variable.

Table 4.3 Electric constants of lossy media.

	Relative permittivity	Conductivity [S/m]	Density [kg/m^3]
Skin	47.0	1.00	1000.0
Fat	5.0	0.09	900.0

Figure 4.7 shows the SAR distributions when the coaxial-slot antenna (parameters of the antenna are shown in Table 4.1.) is inserted into three types of multilayered media. Here, the SAR observation line is shown in Fig. 4.7 (a). The SAR values are normalized with a net input power of 1 W. In each case, peak value of the SAR near the tip of the antenna does not change so much and the tip heating as an important property of the interstitial antenna is satisfied. There are discontinuities in the SAR values at the boundaries between the media. It is caused by the discontinuous change of the electric field normal at the boundary surface (E_z in this case) and the sudden change of σ / ρ (in

Eq. (2.1)) at the time of computing the SAR due to substantial changes in the electric constants of the medium.

When the thickness of the fat layer is increased, the SAR value in the skin layer is increased, although the SAR values in the fat layer changes little. It is also found that the SAR values in the muscle from the position of the slot (z =50 mm) to the position below the fat layer increases as the thickness of the fat layer is increased. According to [13], in the homogeneous medium, the SAR value from the surface to the slot increases if L_{ts} (distance from the tip of the antenna to the center of the slot) > D_t / 2 (half of the antenna insertion depth). In this case, however, the antenna insertion depth D_t becomes effectively smaller as the thickness of the fat layer becomes larger because the electrical properties of the fat layer are closer to those in air than those in other media.

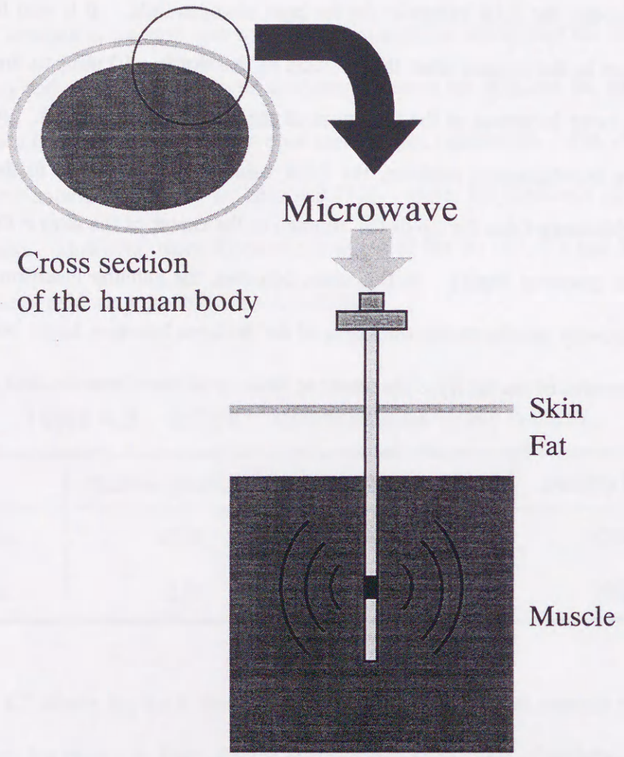

Fig. 4.6 Multilayered medium for calculation.

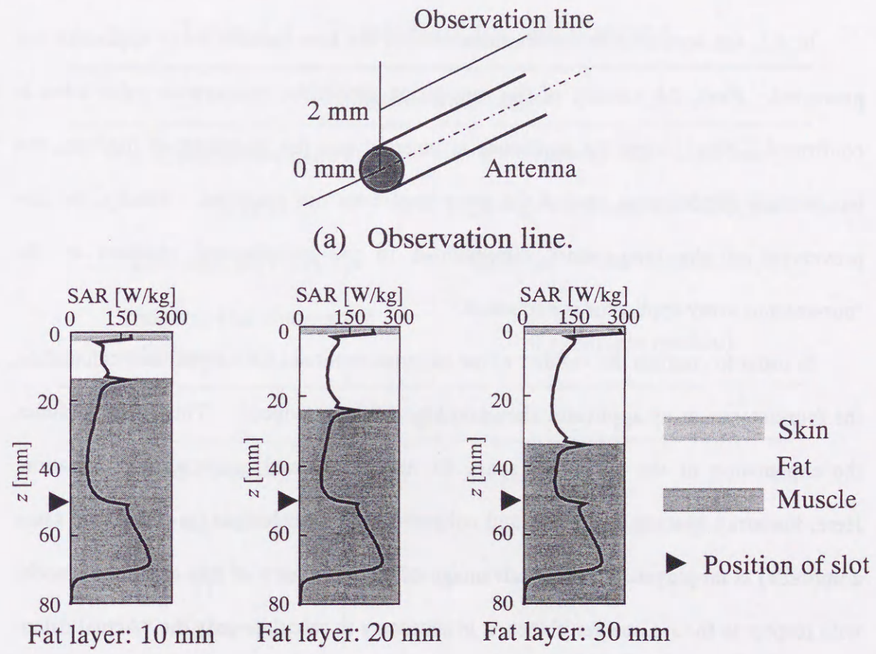

Fig. 4.7 SAR distributions around the coaxial-slot antenna in the multilayered medium.

4.3 Temperature distributions of the array applicator

4.3.1 Validation of calculation model

In 4.3, the temperature distributions around the four-antenna array applicator are presented. First, the validity of the calculation model for temperature calculation is confirmed. Next, when the applicator is inserted into the multilayered medium, the temperature distributions around the array applicator are analyzed. Finally, the improvement of the temperature distributions in the multilayered medium of the four-antenna array applicator is explained.

In order to confirm the validity of the calculation model for temperature calculation, the four-antenna array applicator shown in Fig. 4.8 is introduced. This figure includes the explanation of the calculated space for the FDTD and temperature calculation. Here, the array spacing is 20 mm and coherent feeding technique (in-phase and same amplitude) is employed. Taking advantage of the symmetry of this calculated model with respect to the *x*-*z* and *y*-*z* planes, it is necessary to calculate only the "Actual calculated space" in Fig. 4.8.

The temperature distributions around the array applicator are measured by the thermographic method shown in Section 3.2. In this system, a microwave power divider with four-output ports divides the microwave energy from the generator and the muscle-equivalent phantom is employed as a tissue-equivalent material. The net input power of each antenna is 4.71 W and the heating time is 60 s.

Tables 4.4, 4.5, and 4.6 show the parameters for calculation, the thermal constants

of the antenna, and the electric and thermal constants of the muscle-equivalent phantom, respectively.

Table 4.4 Parameters for calculations.

Parameters for calculation	
Size of calculation space (1/4)	$x \times y \times z = 25 \times 25 \times 160$ mm
Cell size	$\Delta x = \Delta y = 0.1$ mm, $\Delta z = 1.0$ mm
Time step (for FDTD) Δt	0.235 ps (from Courant limit)
Time step (for temperature calculation) Δt	1.0 s (implicit method)
Antenna structure	
Feeding frequency	430 MHz
L_{ts}	20.0 mm
D_t	70.0 mm
d_b	1.19 mm
d_c	2.00 mm
t_c	0.35 mm
ε_{rc}	3.50
ε_{ri}	2.03
Array spacing A_s	20 mm

Table 4.5 Thermal constants of the antenna.

	Specific heart c [J/kg·K]	Thermal conductivity κ [W/m·K]	Density ρ [kg/m^3]
Catheter	1674	0.245	1140
Inner dielectric	974	0.272	2200
Conductor (Copper)	385	398	8950

Table 4.6 Electric and thermal constants of the phantom.

Electrical properties	
Relative permittivity ε_r	53.0
Conductivity σ [S/m]	1.41
Thermal properties	
Specific heat c [J/kg·K]	3725
Thermal conductivity κ [W/m·K]	0.55
Density ρ [kg/m^3]	955

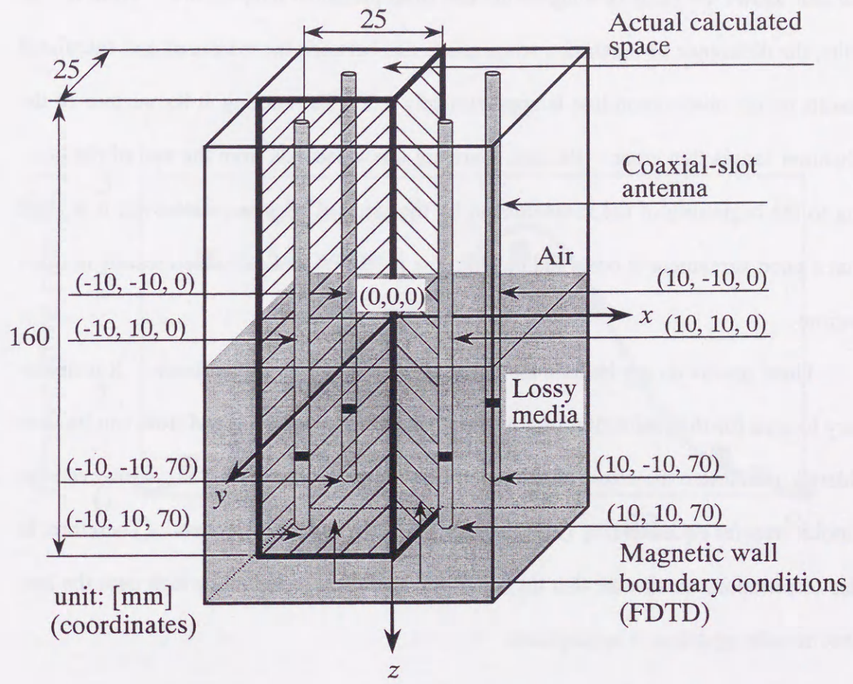

Fig. 4.8 Basic structure of square array applicator composed of four antennas and its calculated space.

Figure 4.9 shows the comparison between the calculated and the measured result. Here, the temperature observation line is the z-axis shown in Fig. 4.8. In Fig. 4.9, the horizontal axis indicates the position on the temperature observation line and the vertical axis shows the value of temperature rise from the initial temperature. From the results, the difference of maximum temperature rise between the measured and calculated results on the observation line is approximately 0.3. The cooling at the surface of the phantom causes that error. Because there are a few seconds from the end of the heating to the beginning of the measurement by the infrared camera. However, it is clear that a good agreement is observed between the measured and calculated results in other regions.

These results do not include the effect of the blood flow in the tissue. It is necessary to wait for the realization of a dynamic phantom by which blood flow can be considered to estimate the effect of the blood flow in the biological tissue. However, the bioheat transfer equation (Eq. (2.2)) is widely used by many researchers. Therefore, in this dissertation, we assume that the use of the analytical technique, which uses the bioheat transfer equation, is appropriate.

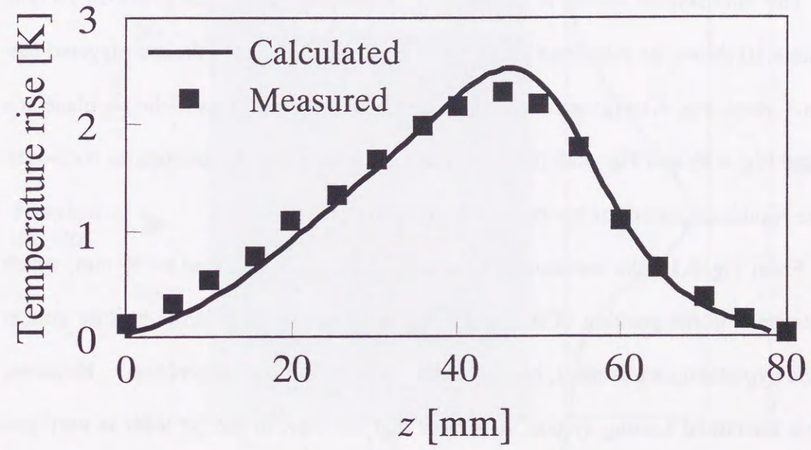

Fig. 4.9 Measured and calculated temperature distribution.

4.3.2 Temperature distributions in the multilayered medium

This section describes the heating characteristics of the array applicator composed of four coaxial-slot antennas. First, the SAR distribution of the array applicator in the multilayered medium is explained. Then, the temperature distributions in the medium are presented.

The multilayered model is the same as the model used in the previous section. Figure 4.10 shows the calculated result of the SAR distributions in the multilayered medium. Here, Fig. 4.10 (a) is a three dimensional SAR distributions in the x-z plane at y =0 (see Fig. 4.8), and Fig. 4.10 (b) is a two dimensional SAR distributions on the z-axis. These results are normalized with a net input power of 1 W.

From Fig. 4.10, the maximum value of the SAR appears around z =50 mm, which corresponds to the position of the slots. In the conventional external heating system for the hyperthermia treatment, heating of the fat layer is a serious problem. However, in this interstitial heating system, it is clear that the SAR in the fat layer is very low compared with the maximum value. This result comes from the low conductivity of the fat. It is the merit of the interstitial heating system.

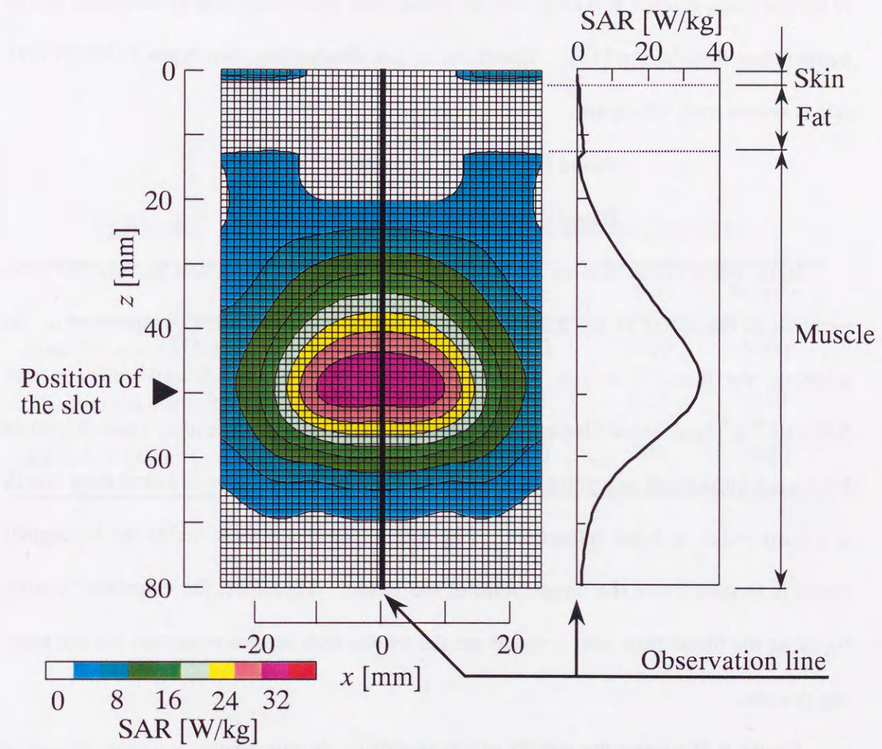

(a) SAR distributions in the observation plane. (b) SAR distributions on the observation line.

Fig. 4.10 SAR distributions in the multilayered medium.

Next, the temperature distributions around the array applicator are calculated by substituting the result of the SAR distributions to the bioheat transfer equation. Table 4.7 shows the thermal constants of the media for the multilayered medium. According to the previous studies, it is clear that the blood flow rate causes a large influence on the temperature distribution [15]. Therefore, in this dissertation, two types of blood flow rate is considered, which are

Blood flow rate A: $F = 8.30\times10^{-6}$ m^3/kg·s,

Blood flow rate B: $F = 4.15\times10^{-6}$ m^3/kg·s.

Here, the specific heat of the blood c_b, the density of the blood ρ_b, and the temperature of the blood T_b are 3,960 J/kg·K, 1,060 kg/m^3, and 37.0 °C, respectively. In addition, the blood flow rate F of the skin and the fat are 1.67×10^{-5} m^3/kg·s and 5.00×10^{-7} m^3/kg·s, respectively [16]. According to some references, various values have been introduced as a value of the blood flow rate. The value of blood flow rate A is a large value in some references. The role of the blood flow inside the biological tissue is to cool down the temperature of the tissue. Therefore, the calculated results by using the blood flow rate A and B are the results with serious condition for the heating devices.

Figure 4.11 shows the results of calculations. In this figure, a region of $x<0$ is displayed for symmetrical structure. Fig. 4.11 (a) shows the transition of the temperature at the temperature observation point 1 explained in Fig. 4.12. Figure 4.11 (b) shows the three dimensional temperature distributions in the x-z plane at y =0 (see Fig. 4.8). In this calculation, the heating time is 600 s and the net input power of each antenna is 10 W (40 W for the array applicator). The initial temperature of the tissue is 37.0 °C.

Table 4.7 Thermal constants of the media [12], [14].

	Skin	Fat	Muscle
Specific heat c [J/kg·K]	3500	2300	3500
Thermal conductivity κ [W/m·K]	0.50	0.22	0.60
Density ρ [kg/m^3]	1000	900	1020

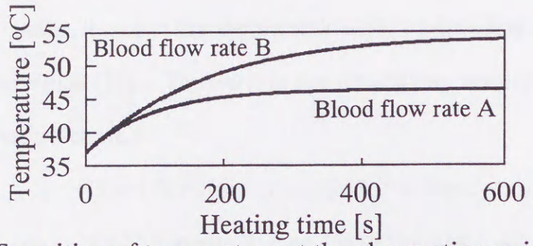

(a) Transition of temperature at the observation point 1.

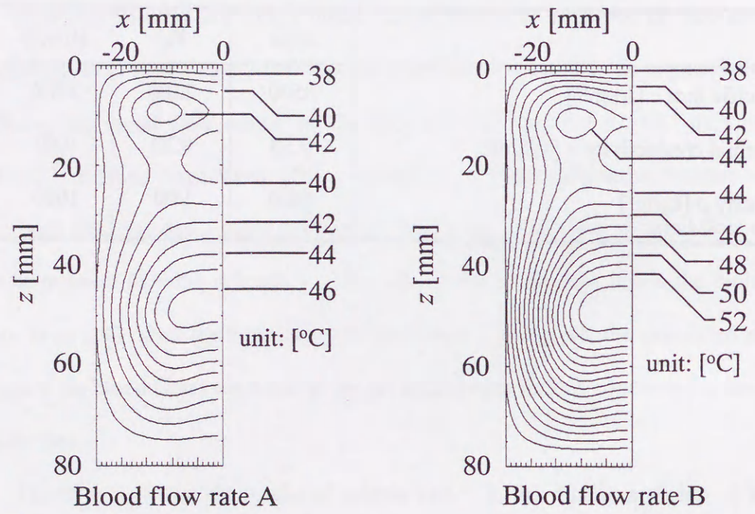

Fig. 4.11 Calaulated results of the temperature distributions in the multilayered medium.

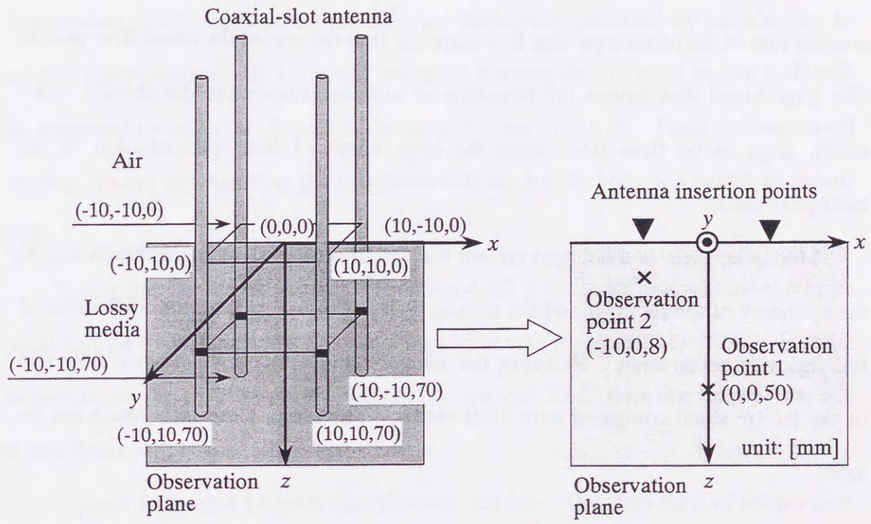

Fig. 4.12 Observation points of temperature.

From Fig. 4.11, the maximum temperature appears at the center of the array applicator i. e. z =50 mm (slot position of each antenna), x =0. The values of maximum temperature are 46 °C (blood flow rate A) and 53 °C (blood flow rate B). By comparing the result of blood flow rate A and B, it is confirmed that the gradient of temperature of the blood flow rate A is larger than the one of the blood flow rate B. Because the contour line of the blood flow rate B is narrower than the one of the blood flow rate A. The large blood flow causes the formation of uniform temperature distribution. Because, large blood flow rate means the large effect of heat transportation in the biological tissue.

Moreover, there is a hot spot around the x =-10 mm, z =10 mm corresponding to the boundary of the fat layer and the muscle layer. From Fig. 4.10, the SAR value of this region is not so large. However, the thermal conductivity and the blood flow rate of the fat are small compared with other media. Therefore, these facts cause the results.

4.3.3 Improvement of temperature distributions in the multilayered medium

In the previous section, calculated results of the array applicator, which has hot spot near the medium boundary, were presented. In this section, the improvement of temperature distributions in the multilayered medium is presented by introducing the on-off feeding control. In the actual treatment, the temperature in the human body will be measured by using the interstitial thermoprobe (see Fig. 1.3). Therefore, the on-off feeding control by observing the temperature in the human body is a useful technique [15].

In this time, observation point 1 (see Fig. 4.12) is set as the temperature reference point and the temperature at this point is kept within the range of 43 to 45 °C. In order to investigate the effect of the blood flow, two types of blood flow rate (blood flow rate A and B) are also employed.

Figures 4.13 and 4.14 show the calculated results. The transitions of temperature are shown in (a) of each figure. Here, the observation point 2 is the point for which the temperature rise was observed in the fat layer without on-off feeding control. Moreover, the temperature transition in the observation point 2 without the feeding control is displayed for comparison. In addition, the three dimensional temperature distributions after heating 600 s are shown in (b) of each figure.

From Figs 4.13 and 4.14, it is clear that the maximum temperature in the observation plane (see 4.12) is 45 °C or less with on-off feeding control. In addition, it is confirmed that the gradient of temperature in the observation plane becomes smaller with on-off feeding control from the comparison between the blood flow rate A of Fig. 4.11

(b) and Fig. 4.13 (b) or blood flow rate B of Fig. 4.11 (b) and Fig. 4.14 (b). In other words, we may say that conducting the on-off feeding control has a possibility of generating more uniform temperature distribution inside the human body. In the hyperthermic treatment, generating the uniform heating region is required. So, these results are useful for actual treatments.

Moreover, it is recognized that the temperature of the fat layer decreases approximately 1 °C (blood flow rate A) or 4 °C (blood flow rate B) by conducting the on-off feeding control. From these results, we are able to improve the temperature distribution in the multilayered medium without changing the structure of the antenna.

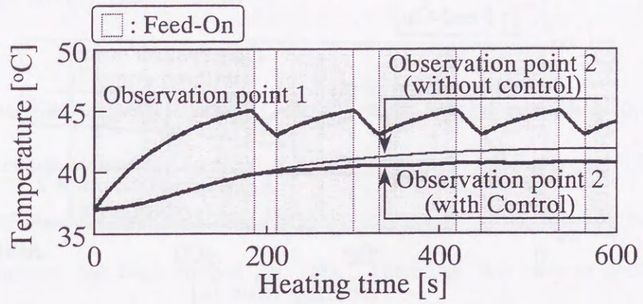

(a) Transition of temperatures.

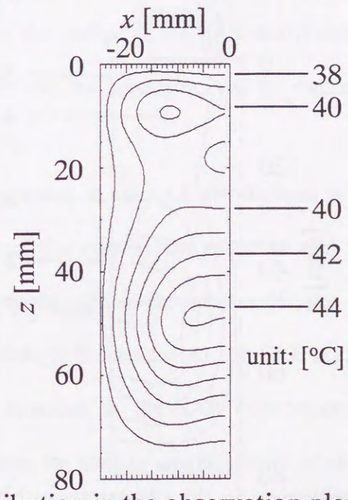

(b) Temperature distribution in the observation plane after heating 600 s.

Fig. 4.13 Calculated results with on-off feeding control (blood flow rate A).

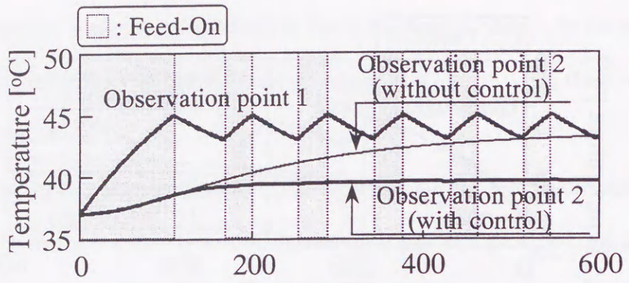

(a) Transition of temperatures.

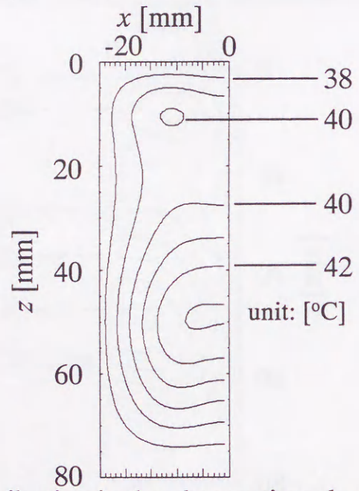

(b) Temperature distribution in the observation plane after heating 600 s.

Fig. 4.14 Calculated results with on-off feeding control (blood flow rate B).

4.4 Control of SAR distributions in the insertion-direction of the array applicator

The interstitial heating techniques, control of the heating patterns in the antenna insertion-direction on inserted applicators have been regarded as important [17]. Until now, the control of the SAR distributions in the antenna insertion-direction concerning the single antenna has been studied [9], [18]. Therefore, this chapter describes the control of the SAR distributions of the array applicator in the antenna insertion-direction. By the way, the control of the SAR distributions of array applicator in the perpendicular direction of the antenna axis is realized by varying the antenna-insertion positions [15].

In order to realize the control of the SAR distributions in the array applicator, the array applicator composed of the coaxial-slot antennas with two slots is introduced. According to the previous study [19], in the array applicator composed of four coaxial-slot antennas with two slots, it is clear that a high SAR region appears between two slots on the longitudinal direction in the SAR observation plane (see Fig. 4.15). Therefore, in this dissertation, the heating characteristics of three types of array applicator as shown in Fig. 4.16 are presented. In these array applicators, the length of L_{ls} (the length from the tip to the nearest slot from the tip) is 5 mm in every case. On the other hand, the length of L_{ts} (the length from the tip to the nearest slot from the feed) is properly changed. In addition, the FDTD method is employed to calculate the SAR distributions around the array applicators. Here, the non-uniform grids are employed for the calculation and conducted small-sized grids only for the antenna portion in x-y

plane. So, in this case, it is possible to calculate in the whole FDTD region without utilizing the symmetrical structure. Table 4.8 shows the parameters for calculations. Moreover, the effectiveness of the controlling method is confirmed by the SAR measurement using the thermographic method.

Table 4.8 Parameters for calculations.

Parameters for calculation			
Size of calculation space	$x \times y \times z = 40 \times 40 \times 160$ mm (Type A, B) $x \times y \times z = 60 \times 40 \times 160$ mm (Type C)		
Minimum cell size	$\Delta x = \Delta y = 0.1$ mm, $\Delta z = 1.0$ mm		
Time step (for FDTD) Δt	0.235 ps (from Courant limit)		
Antenna structure			
Feeding frequency	430 MHz		
D_t	70.0 mm		
d_b	1.19 mm		
d_c	2.00 mm		
t_c	0.35 mm		
ε_{rc}	3.50		
ε_{ri}	2.03		
Array spacing A_s	20.0 mm		
	Type A	Type B	Type C
L_{ls}	5, 5 mm	5, 5 mm	5, 5, 5 mm
L_{ts}	15, 25 mm	15, 35 mm	15, 25, 35 mm

Figure 4.17 shows the calculated results. Here, the SAR values are normalized with a net input power of 4 W (net input power of each antenna is 1 W). By comparing the Fig. 4.17 (a) and (b), it is obvious that the position of the two slots is reflected in the SAR distributions around the array applicators. In other words, the SAR distributions for the large interval of two slots are wide in the antenna insertion-direction and the SAR distributions are narrow for the small interval. This tendency is also observed in the array applicator composed of six antennas shown in Fig. 4.17 (c).

Figure 4.18 shows the measured SAR distributions around the array applicator type B. Here, the net input power of the array applicator is 36.6 W and heating time is 30 s. However, in the Fig. 4.18, the SAR values are normalized with a net input power of 4 W. By comparing the Fig. 4.17 (b) and Fig. 4.18, a good agreement is observed between the calculated and the measured result. Therefore, the control of the SAR distributions in the antenna insertion direction by varying the position of two slots is a useful technique.

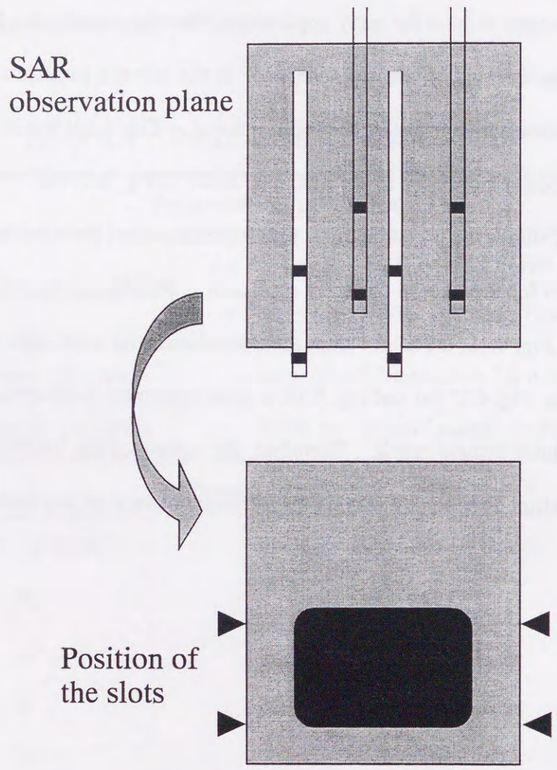

Fig. 4.15 Array applicator composed of four coaxial-slot antennas with two slots.

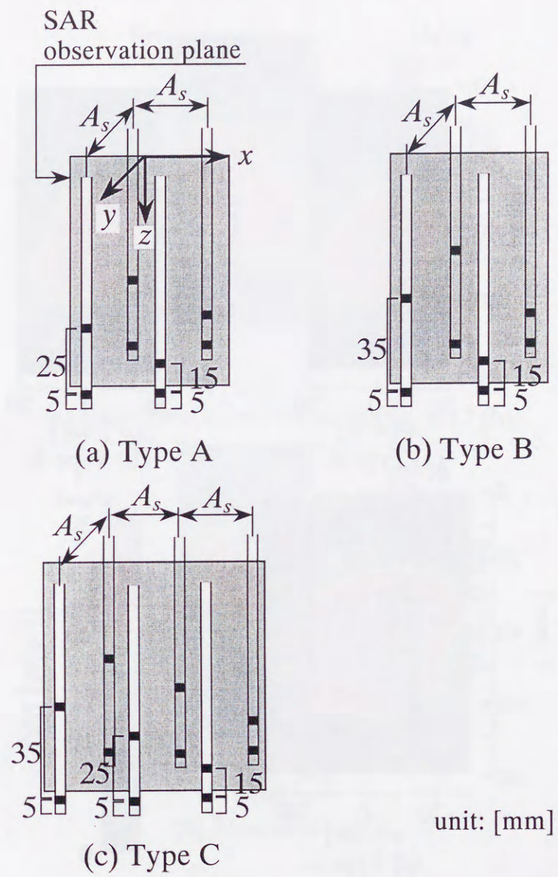

Fig. 4.16 Three types of array applicator composed of four or six coaxial-slot antennas.

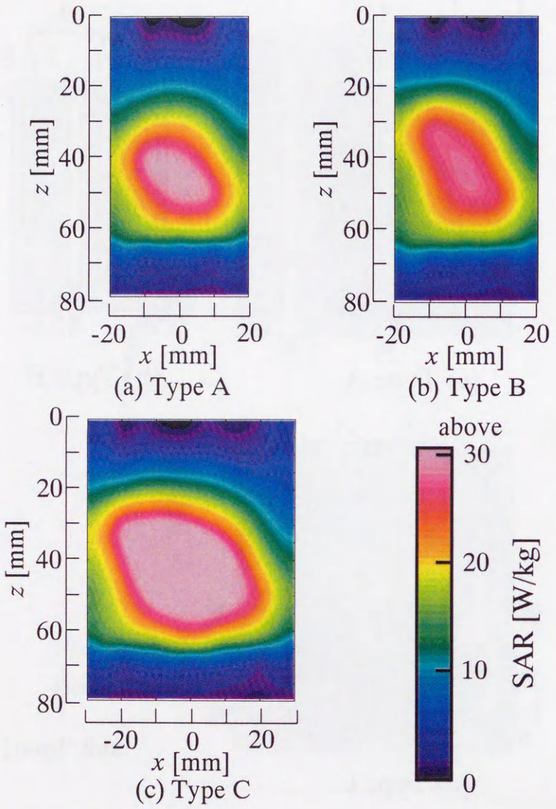

Fig. 4.17 Calculated results of three types of array applicators.

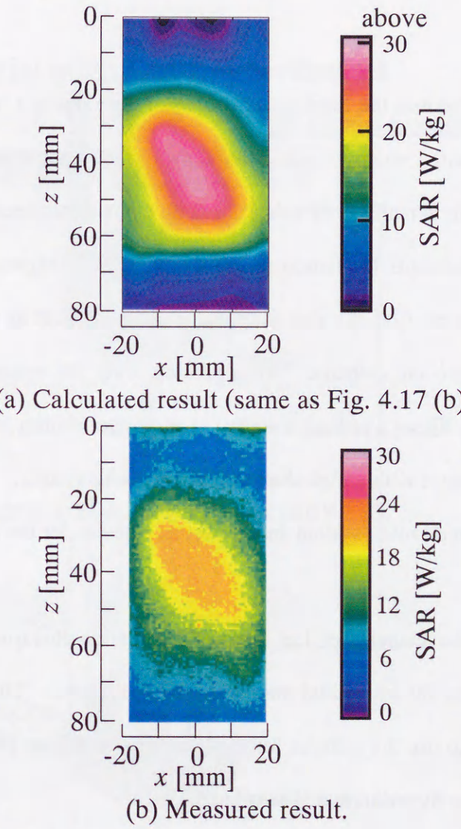

Fig. 4.18 Comparison between the calculated and the measured results.

4.5 Treatment system by combining the interstitial microwave hyperthermia and the interstitial radiation therapy

This chapter describes the fundamental study of developing a treatment system by combining the interstitial microwave hyperthermia and the interstitial radiation therapy. This treatment system is realized by using the same catheter between the interstitial hyperthermia and the interstitial radiation therapy. Figure 4.19 shows the scheme of this system. In this system, first, the thin microwave antennas such as the coaxial-slot antenna are inserted into the catheter. After heating, only the antennas are pulled out from the catheters. Then, a radiation source such as the iridium 192 is automatically inserted into the catheter with a high dose rate afterloading system. Figure 4.20 shows the high dose rate afterloading system and the actual catheter for the interstitial radiation therapy.

Here, we use the catheter of the interstitial radiation therapy for the treatment. The catheter is not for the interstitial microwave hyperthermia. Therefore, in this section, the possibility to use the catheter for the interstitial radiation therapy as that of the interstitial microwave hyperthermia is examined.

First, the heating characteristics of single antenna with catheter for the radiation therapy are examined. Here, the feeding frequency is assumed to be 2450 MHz, which is good for localized heating. Next, the heating characteristics of the array applicator composed of three coaxial-slot antennas are described. We assume that this array applicator will be the minimum unit for structuring more large-scale array applicator [15].

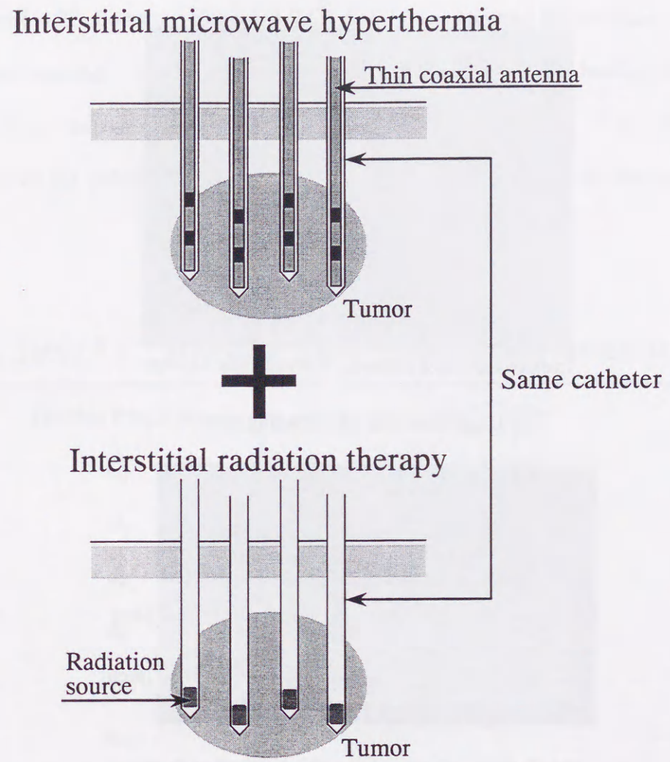

Fig. 4.19 Combined therapy of the interstitial microwave hyperthermia and the interstitial radiation therapy.

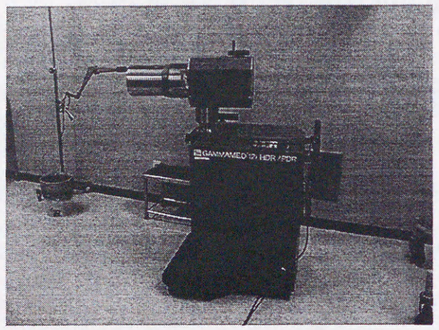

Ichikawa General Hospital, Tokyo Dental College

(a) High dose rate afterloading system.

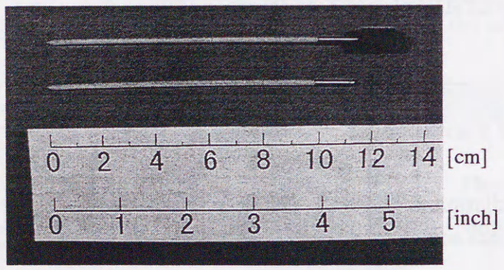

(b) Catheters for the interstitial radiation therapy.

Fig. 4.20 Treatment system of the interstitial radiation therapy.

Figure 4.21 shows the picture of the coaxial-slot antenna with a catheter for the interstitial radiation therapy. In addition, the Table 4.9 shows the structural parameters of the antenna.

Figure 4.22 shows the measured SAR distributions around the antenna by the thermographic method. Here, net input power of the antenna and the heating time are 35 W and 30 s, respectively. From this result, the heating ability of the coaxial-slot antenna with the catheter for the interstitial radiation therapy is good for the treatments.

Table 4.9 Structural parameters for measurements.

Feeding frequency	2450 MHz
L_{ts}	5.0 mm
D_t	50.0 mm
d_b	1.19 mm
d_c	1.98 mm
t_c	0.40 mm
ε_{rc}	–
ε_{ri}	2.03

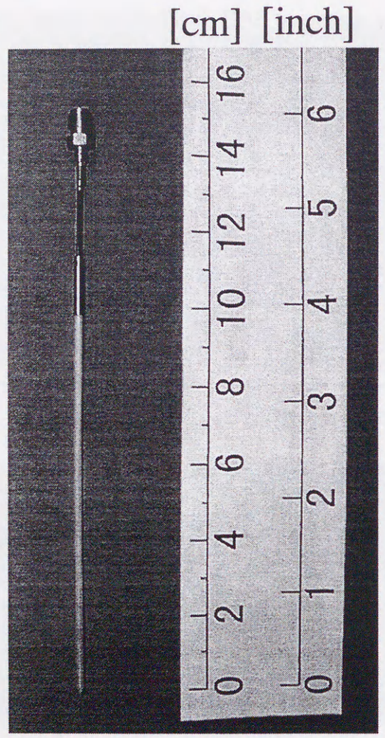

Fig. 4.21 Picture of the coaxial-slot antenna with the catheter for the interstitial radiation therapy.

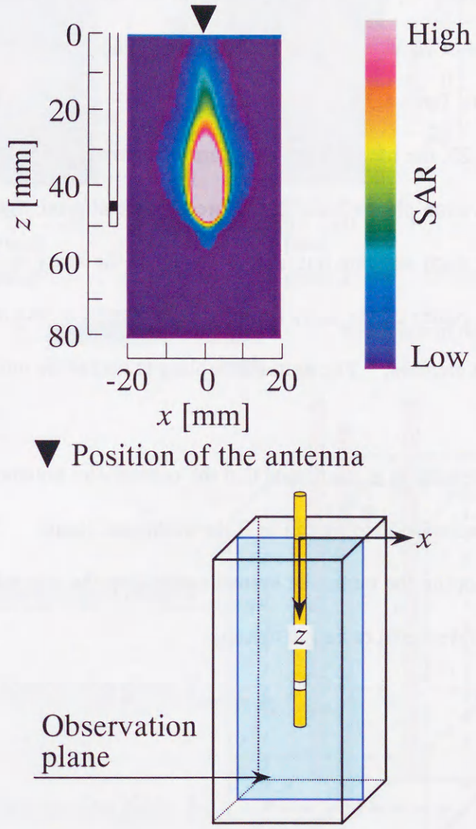

Fig. 4.22 Measured SAR distribution of the coaxial-slot antenna with the catheter for the interstitial radiation therapy.

Figure 4.23 shows the measured SAR distributions of the array applicator composed of three coaxial-slot antennas with the catheter for the interstitial radiation therapy. Here, the array spacing A_s, the net input power of the array applicator and the heating time are 20 mm, about 70 W and 30 s, respectively. The structural parameters of each antenna are shown in Table 4.9.

From Fig. 4.23, the high SAR regions are recognized at around the tip of the antennas in the observation planes 1 and 2. Moreover, we observe that high SAR regions exist not only near each antenna but also at center of the array applicator. The high SAR regions at the center of the array applicator are caused by the mutual coupling between each antenna element. The mutual coupling is useful for uniform heating in the human body.

From these results, it is confirmed that the coaxial-slot antennas with the catheter for the interstitial radiation therapy can heat the biological tissue. Therefore, there is a possibility of developing the treatment system combining the interstitial microwave hyperthermia and the interstitial radiation therapy.

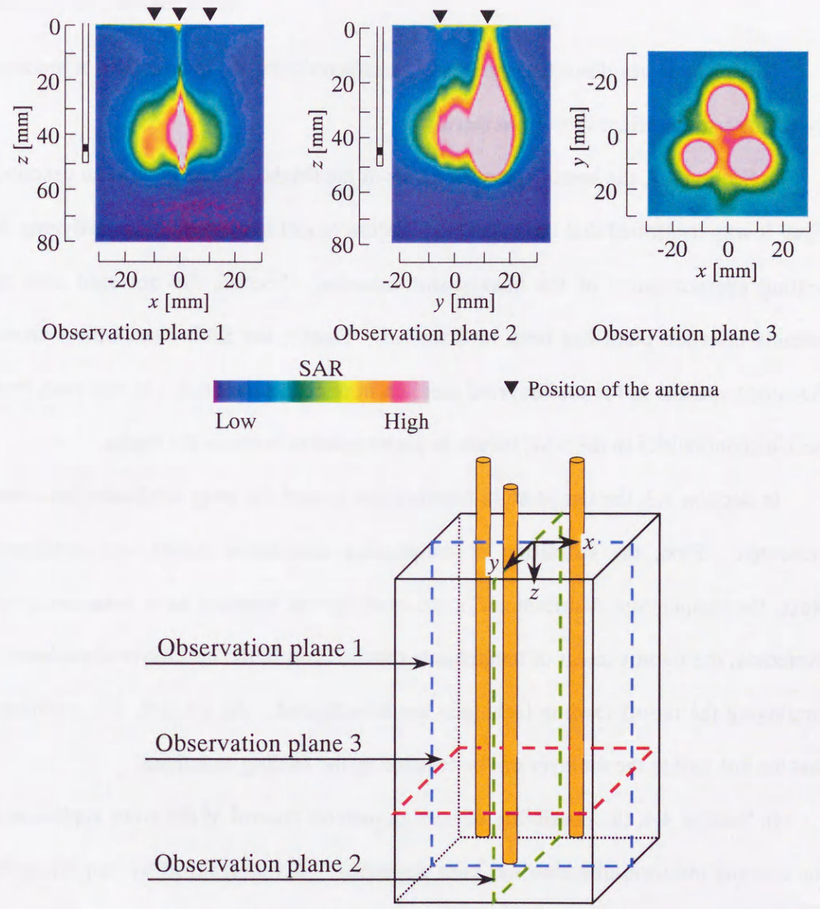

Fig. 4.23 Measured SAR distributions of the array applicator composed of three coaxial-slot antennas with the catheter for the interstitial radiation therapy.

4.6 Conclusions in this chapter

This chapter has described the heating characteristics of the coaxial-slot antennas for the interstitial microwave hyperthermia.

In Section 4.2, the heating characteristics of the single antenna have been described. First, it was confirmed that the FDTD calculation model is useful for the analyzing the heating characteristics of the coaxial-slot antennas. Second, the hot spot near the antenna insertion point has been investigated. Finally, the SAR distributions around the single antenna in the multilayered medium have been presented. In this case, there were discontinuities in the SAR values at the boundaries between the media.

In Section 4.3, the temperature distributions around the array applicator have been presented. First, the validation of temperature calculation model was confirmed. Next, the temperature distributions in the multilayered medium have been described. Moreover, the improvement of temperature distributions in the multilayered medium by employing the on-off feeding technique has investigated. As a result, it is confirmed that the hot spot in the fat layer can be reduced by the feeding technique.

In Section 4.4, the possibility of heating patterns control of the array applicator to the antenna insertion-direction has been described. It was realized by employing the coaxial-slot antennas with two slots. The technique is useful for actual treatments.

In Section 4.5, the fundamental study for developing the treatment system combining the interstitial microwave hyperthermia and the interstitial radiation therapy was explained. We found that the heating ability of the coaxial-slot antenna with the catheter for the interstitial radiation therapy is good for the treatments.

The confirmation of effectiveness of the antennas by the animal experiments is necessary as a further study.

References in Chapter 4

[1] K. Saito and K. Ito, "Study on SAR distribution of coaxial-slot antenna for interstitial microwave hyperthermia using FDTD method," Transactions of the IEICE, vol. J82-B, no. 2, pp. 276-282, 1999 (in Japanese).

[2] K. Saito, O. Nakayama, L. Hamada, and K. Ito, "Analysis of temperature distributions generated by square array applicator composed of coaxial-slot antennas for," Transactions of the IEICE, vol. J82-B, no. 9, pp. 1730-1738, 1999 (in Japanese).

[3] K. Saito, L. Hamada, H. Yoshimura, and K. Ito, "Control of heating pattern to the insertion direction in array applicator for interstitial microwave hyperthermia," Japanese Journal of Hyperthermic Oncology, vol. 15 (suppl.), pp. 304-305, Sep. 1999 (in Japanese).

[4] Y. Akao, "*Fundamentals of electromagnetic compatibility*," Institute of Electrical, Information and Communication Engineers, Tokyo, 1991 (in Japanese).

[5] C. C. Johnson and A. W. Guy, "Nonionizing electromagnetic wave effects in biological materials and systems," Proceedings of IEEE, vol. 60, no. 6, pp. 692-719, 1972.

[6] T. Uno, "*Finite difference time domain method for electromagnetic field and antenna analyses*," Corona publishing, Tokyo, 1998 (in Japanese).

[7] B. C. Wadell, "*Transmission line design handbook*," Artech House, Norwood, 1991.

[8] T. Schmid, O. Egger, and N. Kuster, "Automated E-field scanning system for dosimetric assessments," IEEE Transactions on Microwave Theory and Techniques, vol. 44, no. 1, pp. 105-113, 1996.

[9] L. Hamada, K. Saito, H. Yoshimura, and K. Ito, "Dielectric-loaded coaxial-slot antenna for interstitial microwave hyperthermia: longitudinal control of heating patterns," International Journal of Hyperthermia, vol. 16, no. 3, pp. 219-229, 2000.

[10] M. S. Wu, L. Hamada, K. Ito, and H. Kasai, "Effect of a catheter on SAR distribution around interstitial antenna for microwave hyperthermia," IEICE Transactions on Communications, vol. E-78C, no. 11, pp. 1624-1631, 1995.

[11] M. S. Wu, "Study on the coaxial-slot antenna for interstitial microwave hyperthermia," Ph. D. dissertation at Chiba University, Chiba, Japan, Jul. 1995 (in Japanese).

[12] H. N. Kritikos and H. P. Schwan, "Formation of hot spots in multilayer spheres," IEEE Transactions on Biomedical Engineering, vol. BME-23, no. 3, pp. 168-172, 1976.

[13] K. Saito, T. Kitada, L. Hamada, and K. Ito, "Study on heating pattern of multiple coaxial-slot antenna for interstitial microwave hyperthermia by varying slot arrangement," Technical report of IEICE, vol. A·P96-126, pp. 49-56, Jan. 1997 (in Japanese).

[14] J. Wang and O. Fujiwara, "FDTD computation of temperature rise in the human head for portable telephones," IEEE Transactions on Microwave Theory and Techniques, vol. 47, no. 8, pp. 1528-1534, 1999.

[15] L. Hamada, "Study on the array applicator for microwave interstitial hyperthermia," Ph. D. dissertation at Chiba University, Chiba Japan, Feb. 2000.

[16] P. M. Van Den Berg, A. T. De Hoop, A. Segal, and N. Praagman, "A computational model of the electromagnetic heating of biological tissue with application to hyperthermic cancer therapy," IEEE Transactions on Biomedical Engineering, vol. BME-30, no. 12, pp. 797-805, 1983.

[17] T. Z. Wong, J. W. Strohben, K. M. Jones, J. A. Mechling, and B. S. Trembly, "SAR patterns from an interstitial microwave antenna-array hyperthermia system," IEEE Transactions on Microwave Theory and Techniques, vol. 34, no. 5, pp. 560-567, 1986.

[18] K. Saito, T. Kitada, L. Hamada, and K. Ito, "Study on heating pattern of multiple coaxial-slot antenna for interstitial microwave hyperthermia by varying slot arrangement," Technical report of IEICE, vol. A·P96-126, pp. 49-56, Jan. 1997 (in Japanese).

[19] O. Nakayama, "Control of heating characteristics to the direction to the insertion depth in coaxial-slot antenna array for interstitial microwave hyperthermia," Master's thesis at Chiba University, Chiba Japan, Feb. 1999 (in Japanese).

Chapter 5

Improvement on the coaxial antennas for the microwave coagulation therapy

5.1 Introduction

This chapter describes the improvement of heating characteristics of the coaxial antennas for the microwave coagulation therapy. As mentioned earlier, there are two major problems in the conventional antenna for the MCT. First, in the conventional antenna, the size of coagulated region is insufficient, especially in the perpendicular direction of the antenna axis [1]. Second, the length of the coagulated region becomes longer into the antenna insertion direction [2]. In order to solve the first problem, an array applicators composed of small number of the antennas is introduced. Moreover, the second problem is overcome by employing the coaxial-dipole antenna.

First, in Section 5.2, the validity of the calculation model is confirmed. Here, the temperature dependence on the electric constants of the biological tissue is included. After the validity, in Section 5.3, in order to expand the coagulated region in the perpendicular direction of the antenna axis, the array applicators composed of small number of coaxial-slot antennas are presented. In Section 5.4, the localized heating only around the tip of the antenna is described by employing the coaxial-dipole antenna.

Moreover, in Section 5.5, the heating characteristics of the coaxial-dipole antenna are improved by adjusting the length of the sleeves.

In this chapter, the feeding frequency is assumed to be 2450 MHz. The frequency is one of the ISM (Industrial, Scientific, and Medical) frequencies [3], and is used for the conventional treatment [4].

5.2 Validation of calculation model

5.2.1 Attempt of temperature calculation with temperature-dependent electric constants

During the MCT treatment, the electric constants of the target tissue change because the MCT is a treatment that generates high temperature regions in the tissue to coagulate the cancer cells. In order to simulate the temperature in the tissue accurately, the electric constants of the tissue are measured at various temperatures. The results of the measurement are used for the numerical calculation of the heating characteristics of the antenna.

(1) Measurement of temperature-dependence of the electric constants

Figure 5.1 shows the measurement system of temperature-dependent electric constants of the tissue. In this time, the temperature dependence of the relative permittivity and the conductivity of the liver of pig are measured because the electric constants of the liver of pig are similar to the constants of human body [5]. Measured temperatures range from 20 to 100 °C. The liver of pig is preheated before the measurement by using the water bath for 15 minutes (the measurement temperature is set by the water temperature). After 15 minutes, the electric constants of the liver are measured quickly by using the dielectric measurement system (Hewlett Packard HP85070B dielectric constants measurement system).

Figure 5.2 shows the measured results of the temperature-dependence of the relative permittivity and the conductivity of the liver at 2450 MHz. Here, the number of samples is 15 at each temperature. The error bar at the 60 °C is larger than those of other temperature because the liver tissue begins to coagulate at 60 °C. From Fig. 5.2, both the relative permittivity and the conductivity of the liver decrease while increasing the temperature.

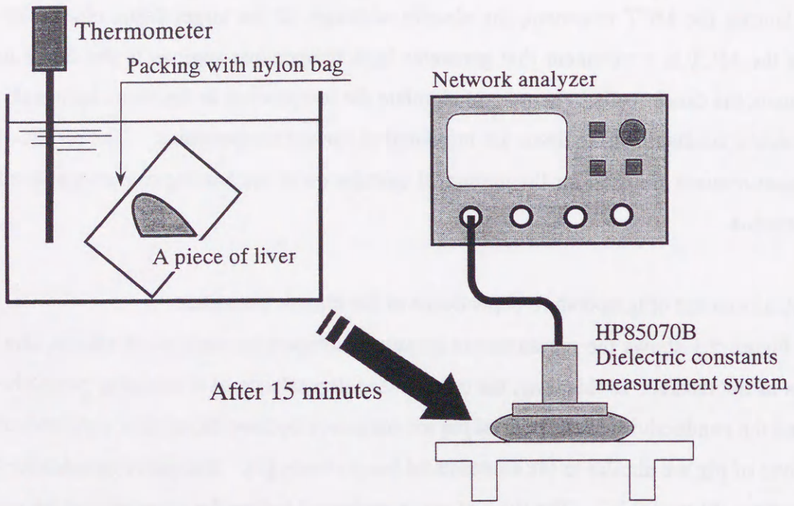

Fig. 5.1 Measurement system for temperature-dependent electric constants of the tissues.

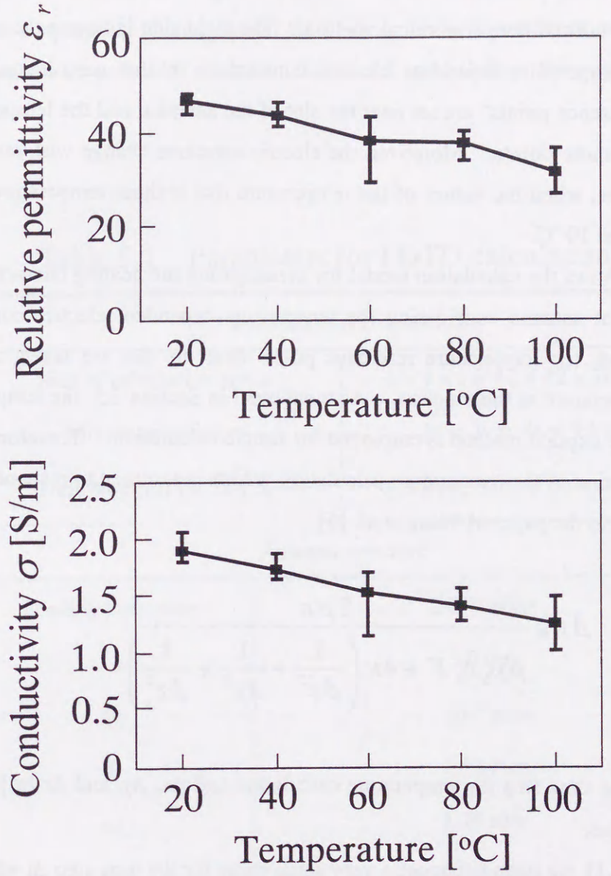

Fig. 5.2 Temperature-dependence of the electric constants of the liver of pig.

(2) Instance of calculation

Figure 5.3 shows the procedure of calculation considering the effect of temperature-dependent electric constants. The left side is identical to the Fig. 2.2 corresponding to the part of normal temperature calculation. The right side indicates the calculation effect of temperature-dependent electric constants. In this calculation, some "temperature reference points" are set near the slot of the antenna, and the temperatures are monitored at these points. Moreover, the electric constants change with respect to these temperatures, when the values of the temperature rise at these temperature reference points exceed 10 °C.

Figure 5.4 shows the calculation model for investigating the heating characteristics of the coaxial-slot antenna considering the temperature-dependent electric constants. In this calculation, ten temperature reference points near the slot are taken, and we monitor the temperature at these points. As mentioned in Section 2.5, the temperature calculation by the explicit method is employed for simple calculation. Therefore, there is a stability criterion of the temperature calculation, which is assumed to respond to Eq. (5.1) by referring to the paper of Wang *et al.* [6]

$$\Delta t \le \frac{2\rho c}{\rho \rho_b c_b F + 4\kappa \left(\frac{1}{\Delta x^2} + \frac{1}{\Delta y^2} + \frac{1}{\Delta z^2} \right)} \tag{5.1}$$

where Δt [s] is the time step for temperature calculation and Δx, Δy, and Δz [m] are the minimum cell sizes.

From Eq. (5.1), we have to choose a very small value for the time step Δt when κ is large. In general, κ in the conductor of the antenna is very large compared with the one of the biological tissue. However, it is impossible to set a very small time step for practical calculation. In this dissertation, the heat transfer in the part of the conductor is assumed to be small because the conductor part is a very small volume. Under this assumption, the antenna portion is replaced to an object having the same material characteristics as the one of the catheter.

The results of temperature calculation in the interstitial applicator show the fact that the very near region of the antenna gets very hot. In this paper, the maximum temperature in the calculation space is supposed to be 100 °C because high temperature causes the evaporation of moisture in the tissue. These assumptions are employed as far as there are no particular remarks. Tables 5.1 and 5.2 show the parameters for calculation.

Table 5.1 Parameters for FDTD calculations.

Parameters for calculation	
Size of calculation space	$x \times y \times z = 42 \times 42 \times 160$ mm
Minimum cell size	$\Delta x = \Delta y = \Delta z = 0.1$ mm
Time step (for FDTD) Δt	0.192 ps (from Courant limit)
Antenna structure	
Feeding frequency	2450 MHz
L_{ts}	5.0 mm
D_t	70.0 mm
d_b	1.19 mm
d_c	1.79 mm
t_c	0.30 mm
ε_{rc}	2.60
ε_{ri}	2.03

Table 5.2 Parameters for temperature calculation [7]-[11].

	Liver	Antenna (catheter)
Specific heat c [J/kg·K]	3600	974
Thermal conductivity κ [W/m·K]	0.5	0.272
Density ρ [kg/m^3]	1060	2200
Blood flow rate F [m^3/kg·s]	5.0×10^{-6}	–
Specific heat of blood c_b [J/kg·K]	3960	–
Density of the blood ρ_b [kg/m^3]	1060	–
Time step (for temperature calculation) Δt	0.005 s (explicit method)*	

* From Eq. (5.1), for temperature calculation, it is necessary to set the time step Δt smaller than 0.019 s. Therefore, in this case, in order to satisfy the stability criterion enough, the time step Δt is assumed to be 0.005 s.

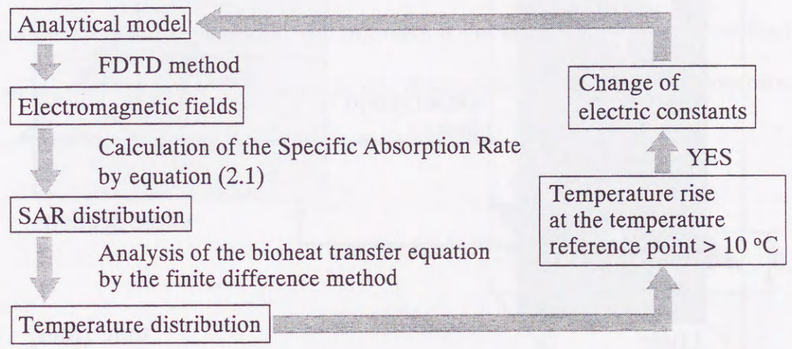

Fig. 5.3 Procedure for calculation considering the temperature-dependent electric constants.

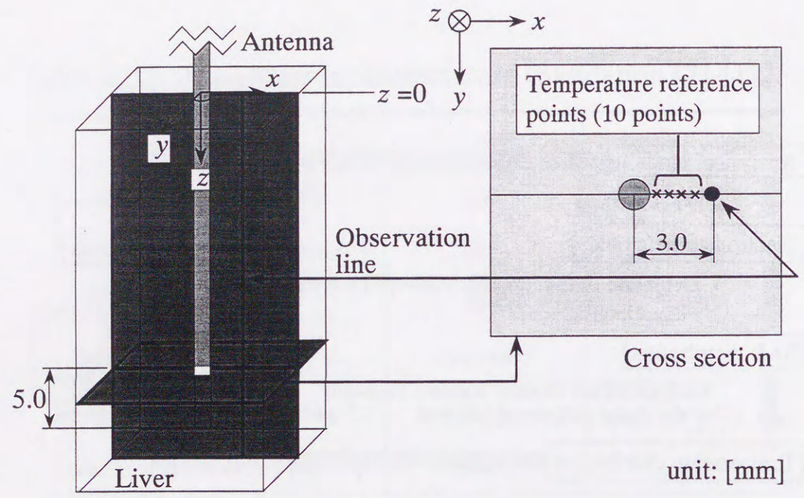

Fig. 5.4 Calculation model for calculating the heating characteristics of the antenna considering the temperature-dependent electric constants.

Figure 5.5 shows the instance of calculation results. Here, the calculated results by conducting the fixed electric constants are shown in the same figure for comparison. In addition, in this result, a change of reflection coefficient of the antenna, which is made by changing the electric constants, is considered. Figure 5.5 (a) shows the SAR distributions on the observation line. The input power of the antenna, the heating time, and the initial temperature of the tissue are 30 W, 60 s, and 37 °C, respectively. The difference between the result of "fixed" and "changed" constants is approximately 10 %. However in this case, from Fig. 5.5 (b), there is not significant difference on the temperature distributions*. Therefore, in this dissertation, the fixed electric constants are employed for calculating the temperature distributions.

* The fixed thermal constants cause that result. However, a good agreement is observed between the calculated and the measured results by using the fixed electric and thermal constants as shown in 5.2.2. Therefore, the use of fixed constants is an appropriate assumption.

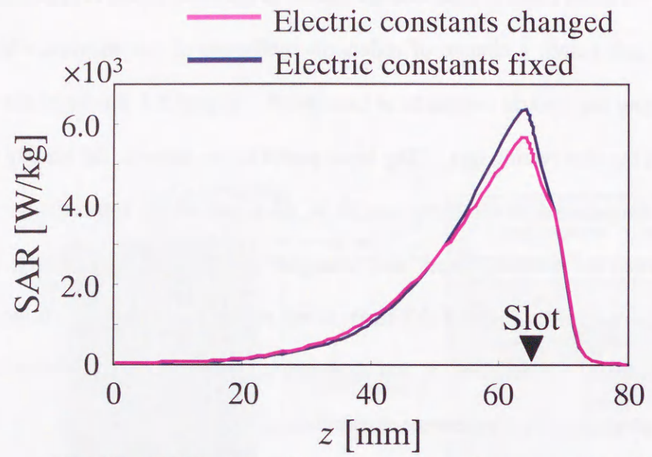

(a) SAR distributions on the observation line.

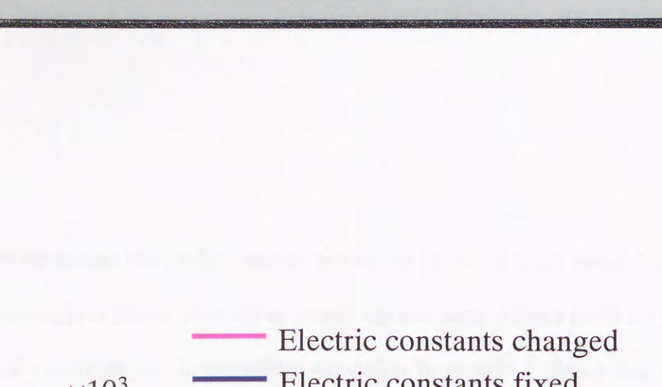

(b) Temperature distributions on the observation line.

Fig. 5.5 Calculated results of heating characteristics by considering the temperature-dependent electric constants.

5.2.2 Validation of calculation model by coagulation experiment

In this section, validity of the calculation model is confirmed by the coagulation experiment using a real biological tissue. The calculation model is shown in Fig. 5.6. Here, the temperature dependence of the electric constants is not considered and the values of Table 5.3 are employed. The values of the other employed parameters appear on Tables 5.3 and 5.4. The parameters in these tables are the value of the human body. However, we adopted the values of a liver of pig for the following reasons: according to our own measurements, the relative permittivity and conductivity of the liver of pig were almost the same values as those of the human body (relative permittivity and conductivity of the liver of pig are 43.66 and 1.73 S/m, respectively.). From [9], the thermal conductivity of the liver of a human is from 0.467 to 0.527 and that of the liver of a pig is 0.528. Therefore, the value of 0.5 is applied as the thermal conductivity of the liver of pig. Moreover, according to our own measurements, the density of the liver of pig had almost the same value as the one of human body.

Figure 5.7 shows the setup of the coagulation experiment for the validation of calculation. In this system, the liver of pig is preheated about 30 °C. Then, the coaxial-slot antenna is placed between two liver blocks. During the coagulation, the net input power is observed by using a power reflection meter (Rohde & Schwarz NRT, NRT-Z44). After heating, the coagulated region on the surface of one piece of the liver block is observed.

Table 5.3 Parameters for FDTD calculations.

Parameters for calculation	
Size of calculation space	$x \times y \times z = 53 \times 53 \times 160$ mm
Minimum cell size	$\Delta x = \Delta y = 0.1$ mm, $\Delta z = 1.0$ mm
Time step (for FDTD) Δt	0.235 ps (from Courant limit)
Antenna structure	
Feeding frequency	2450 MHz
L_{ts}	5.0 mm
D_t	70.0 mm
d_b	1.19 mm
d_c	1.79 mm
t_c	0.30 mm
ε_{rc}	2.60
ε_{ri}	2.03
Biological tissue	
Liver [7]	$\varepsilon_r = 43.03$, $\sigma = 1.69$ S/m

Table 5.4 Parameters for temperature calculation [7]-[11].

	Liver	Antenna (catheter)
Specific heat c [J/kg·K]	3600	974
Thermal conductivity κ [W/m·K]	0.5	0.272
Density ρ [kg/m^3]	1060	2200
Time step (for temperature calculation) Δt	0.01 s (explicit method)*	

* From Eq. (5.1), for temperature calculation, it is necessary to set the time step Δt smaller than 0.019 s. Therefore, in this case, in order to satisfy the stability criterion enough, the time step Δt is assumed to be 0.01 s.

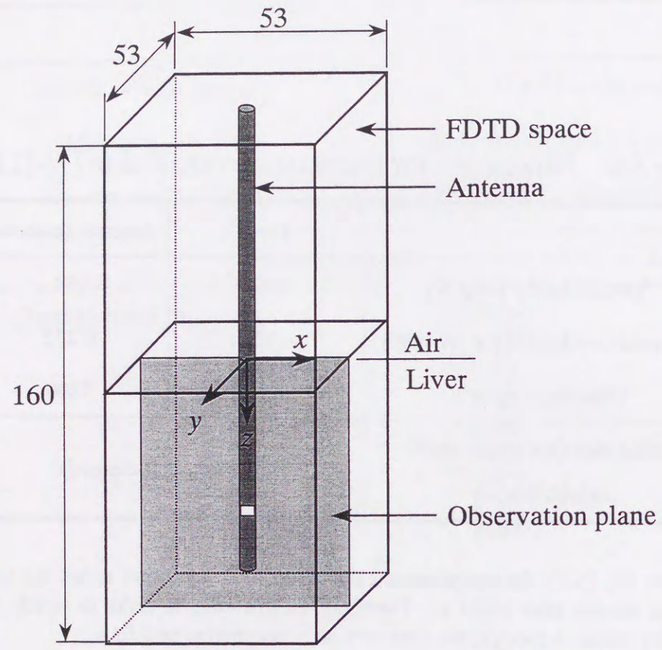

Fig. 5.6 Calculation model for confirmation of the validity.

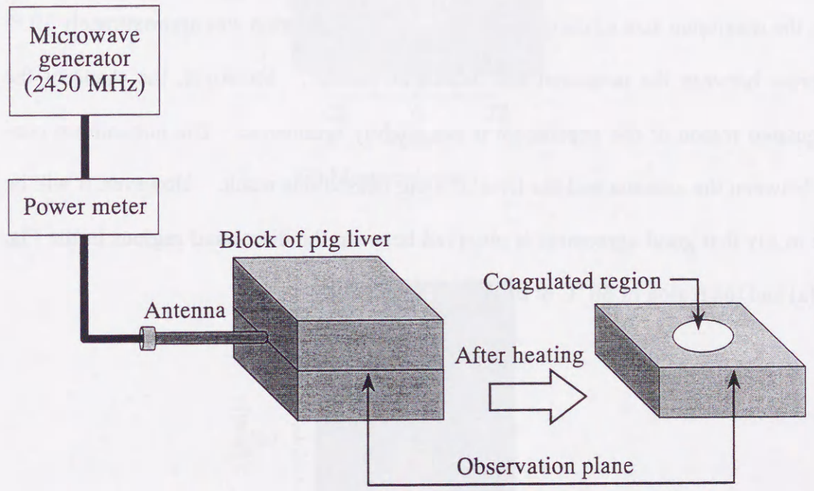

Fig. 5.7 Setup of the coagulation experiment for validation of the calculations.

Figure 5.8 (a) shows the result of the coagulation experiment in the observation plane, and Fig. 5.8 (b) shows the calculated result. Here, the net input power of the antenna and heating time are assumed to be 37.3 W and 90 s, respectively. In Fig. 5.8 (a), the discolored region corresponds to the coagulated region, which reaches 60 °C or more during the experiment. In the experiment, the maximum sizes of the coagulated region of the x- and z- directions were 18.5 and 40.0 mm, respectively. In the calculation, the maximum size of coagulated region in the z-direction was approximately 10 % different between the measured and calculated results*. Moreover, the shape of the coagulated region of the experiment is not slightly symmetric. The nonuniform contact between the antenna and the liver of a pig caused this result. However, it will be able to say that good agreement is observed between the discolored regions in the Fig. 5.8 (a) and the region of 60 °C or more in Fig. 5.8 (b).

* In our own experiments, the coagulation of liver tissue occurs at 60 °C or more. Therefore, in this dissertation, 60 °C is defined as the coagulation temperature.

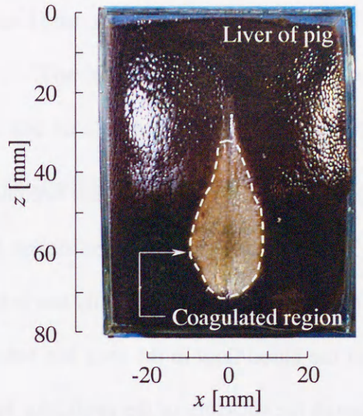

(a) Measured result.

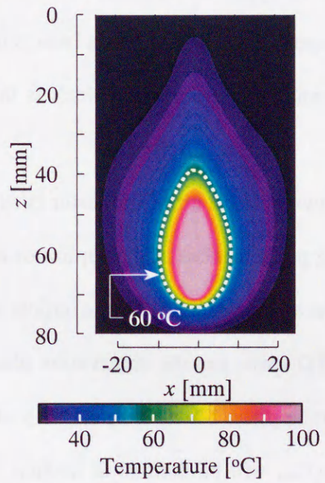

(b) Calculated result.

Fig. 5.8 Validation of calculation.

5.3 Expanding the coagulated region by the array applicator

5.3.1 Array applicator

The clinical side has wished that the coagulated region becomes a sphere of about 3 cm in diameter. However, it is difficult to obtain the sufficient coagulated region in the perpendicular direction of the antenna axis by using only one antenna.

Until now, the intercept of the blood flow in the liver has been investigated to expand the coagulated region, though the structure of the applicator has not been theoretically improved [1]. Therefore, in this section, to expand the coagulated region, the heating characteristics of an array applicator composed of a few coaxial-slot antennas are described by using the computer simulation. As a basic study of an array applicator for the MCT, the two-antenna array applicator, which is the simplest structure, is introduced.

First, the structure of the two-antenna array applicator is explained. Then, the indices for evaluating the heating performances of the applicator are introduced. In particular, the relations between the array spacing and these indices are shown.

Figure 5.9 shows the FDTD space and the observation planes for the two-antenna array applicator. The observation plane 1 is the x-z plane at y =0, the observation plane 2 is the x-y plane at $z = Z_{max}$ (Z_{max} will be defined in Section 5.3.2.), and observation plane 3 is the y-z plane at x =0.

The coagulated region of the two-antenna array applicator with A_s=5, 10, 15, 20, 25, and 30 mm is considered, when the net input power of each antenna P_{net} is 25 or 50

W (total net input power of one antenna is 50 or 100 W.). In the MCT, the input power of one antenna is several tens of Watts, therefore, these values are employed as the input power of the antenna. The initial temperature of the tissue and the heating time are assumed to be 37 °C and 90 s, respectively, by considering the actual treatment. The other parameters for calculation are the same as in Tables 5.3 (except the size of calculation space) and 5.4.

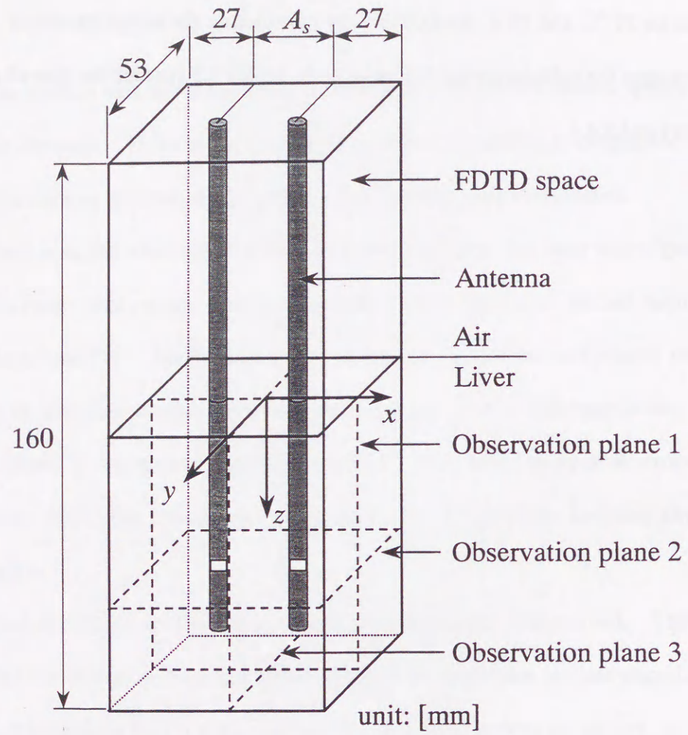

Fig. 5.9 Calculation space and observation planes for two-antenna array applicator.

5.3.2 Expanding the coagulated region by introduction of the indices for evaluating the heating performances

In order to evaluate the heating performances of the array applicators, the following three indices are introduced (see Fig 5.10).

- The length of the continuous area heated over 60 °C or more on the z-axis in observation plane 1. This length is defined as H_{lz}. When the array spacing A_s is sufficiently large and region of 60 °C or more separates into two regions or more, H_{lz} =0.
- The maximum diameter of the continuous area heated over 60 °C or more in observation plane 2. This diameter is defined as H_{lr}. When array spacing A_s is sufficiently large and the region of 60 °C or more separates into two regions or more, H_{lr} =0.
- The position of z where H_{lr} becomes maximum. This position is defined as Z_{max}. However, Z_{max} cannot be defined in the case that H_{lr} =0.

Figure 5.11 shows the calculated results. Figure 5.11 (a) and (b) show the indices H_{lz} and H_{lr}, respectively, for the array spacing A_s over the range of 5-30 mm. Figure 5.11 (c) shows the index Z_{max} where H_{lr} becomes maximum for array spacing A_s over the range of 5-25 mm. From Fig. 5.11 (a), the index H_{lz} becomes maximum at A_s =10 mm, for both values of P_{net}.

In Fig. 5.11 (b), the index H_{lr} decreases monotonously with increasing values of A_s over the range of 5-30 mm when P_{net} =25 W. However, the index H_{lr} has the peak

value at A_s =10 mm when P_{net} =50 W. The index H_{lr} =0 when A_s = 25 mm and P_{net} =25 W or when A_s =30 mm and P_{net} =50 W. Therefore, we assume that each element of the array applicator become independent to these array spacings.

When Z_{max} is small, the effective heating around the tip of the antenna is impossible. However, from Fig. 5.11 (c), Z_{max} takes almost constant values between 55 and 60 mm at both values of P_{net} for A_s over the range from 5 to 25 mm. From this result, the two-antenna array applicator can generate the effective heating region around the tip.

In order to expand the coagulated region in the perpendicular direction of the antenna axis, the array applicators are introduced. Figure 5.12 shows the temperature distributions of the two-antenna array applicator in the observation planes when A_s =10 mm and P_{net} =50 W, because the index H_{lr} was the largest under this condition. In Fig. 5.12, circles of 3 cm in diameter are shown in gray dot line. From Fig. 5.12, the size of region of 60 °C or more covers almost the sphere with the diameter of 3 cm. This result clearly shows that the array applicator expands the coagulated region and is useful for the MCT.

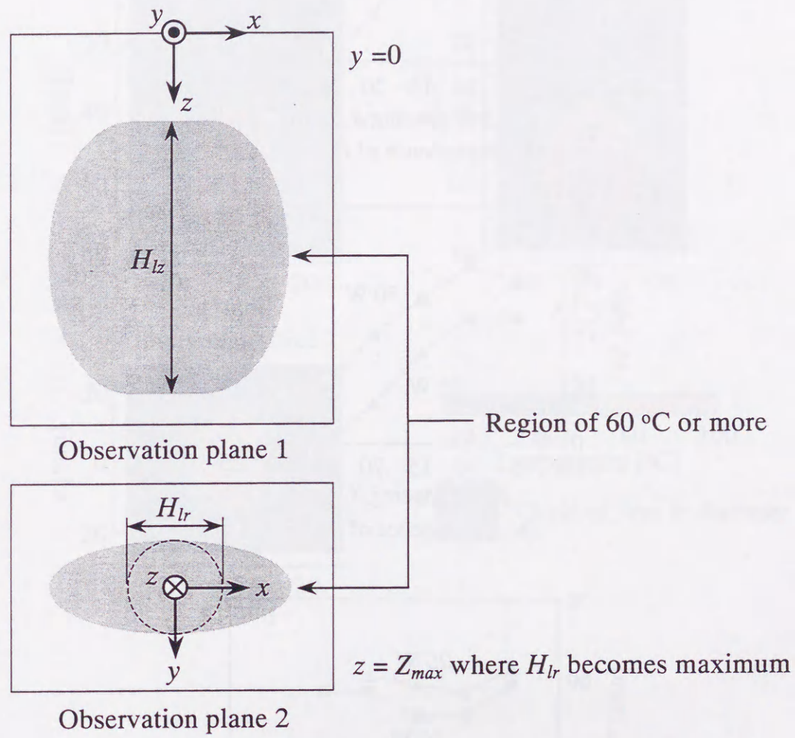

Fig. 5.10 Indices for evaluating the heating performances of the two-antenna array applicator.

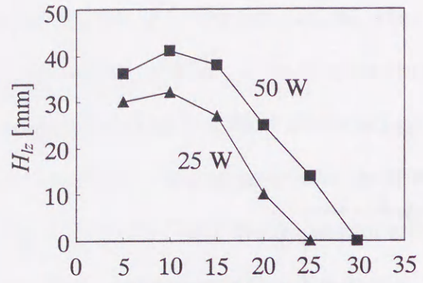

(a) Dependence of H_{lz} on A_s.

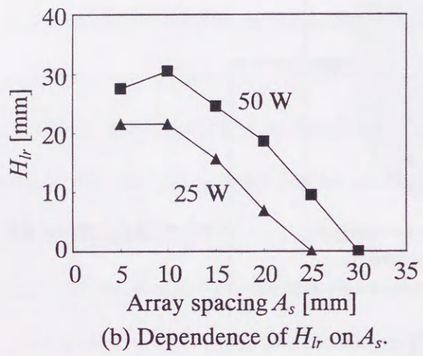

(b) Dependence of H_{lr} on A_s.

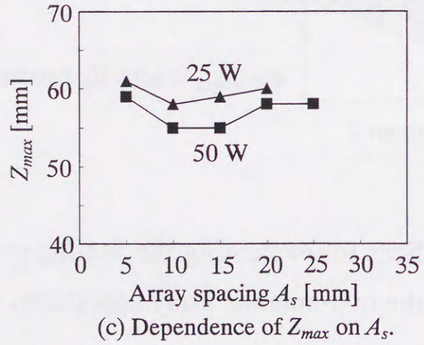

(c) Dependence of Z_{max} on A_s.

Fig. 5.11 Heating performances of the two-antenna array applicator.

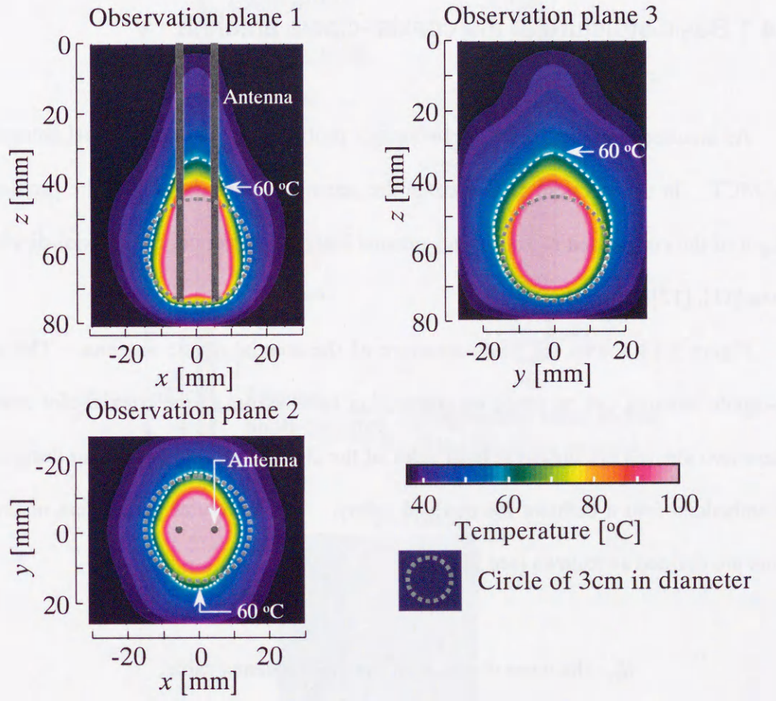

Fig. 5.12 Temperature distributions of the two-antenna array applicator (A_s =10 mm, P_{net} =50 W).

5.4 Introduction of the coaxial-dipole antenna

5.4.1 Basic structure of the coaxial-dipole antenna

As mentioned earlier, there are two major problems in the conventional antenna for the MCT. In this section, to overcome the second problem, which is the problem of length of the coagulated region in the antenna insertion direction, the coaxial-dipole antenna [11], [12] is introduced.

Figure 5.13 shows the basic structure of the coaxial-dipole antenna. The coaxial-dipole antenna can be made by connecting two sleeves to the coaxial-slot antenna. These two sleeves are placed at both sides of the slot. The antenna is also designed to be embedded into a catheter for medical safety. The structural parameters of the antenna are defined as follows (see Fig. 5.13):

d_{bi} : the outer diameter of the inner antenna cable,

d_{bs} : the outer diameter of the sleeve,

d_c : the outer diameter of the catheter,

D_t : the insertion depth,

$2L_d$: the length of the sleeves,

W_{sl} : the width of the slot (in this study, W_{sl} is set to 1.0 mm),

ε_{rc} : the relative permittivity of the catheter,

ε_{ri} : the relative permittivity of the inner dielectric.

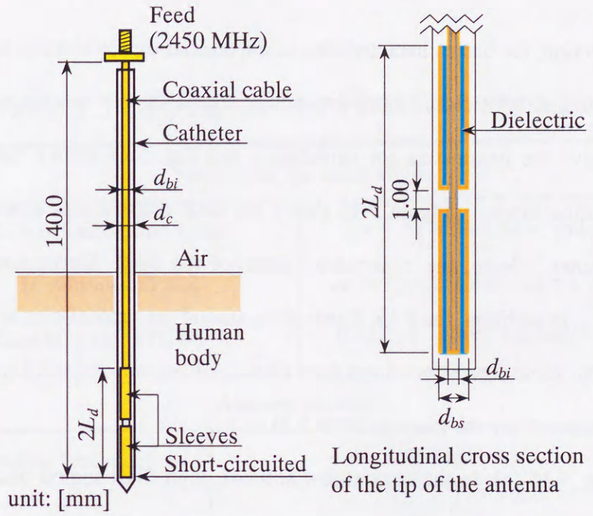

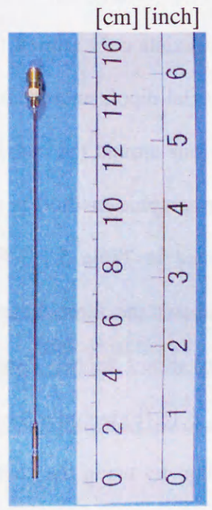

Fig. 5.13 Basic structure of the coaxial-dipole antenna.

5.4.2 Basic characteristics of the coaxial-dipole antenna

In this section, the basic characteristics of the coaxial-dipole antenna are described. First, the calculated SAR distributions around the coaxial-dipole antenna are presented. Table 5.5 shows the parameters for calculation and Fig. 5.14 shows instance of the FDTD calculation model. Figure 5.15 shows the SAR distributions around the coaxial-dipole antenna. Here, the observation plane of the SAR distributions is the x-z plane at y =0. In addition, the SAR distribution around the coaxial-slot antenna is also presented in the same figure for comparison (the L_{ts} of the antenna is 10 mm; the other structural parameters are the same as Table 5.3).

From Fig. 5.15 (a), in the coaxial-slot antenna, high SAR region becomes longer into the antenna insertion direction. However, in Fig. 5.15 (b), high SAR region around the coaxial-dipole antenna exists only around the tip of the antenna. In other words, high SAR region of the coaxial-dipole antenna is located around the two sleeves.

Moreover, the SAR distributions around the coaxial-dipole antenna are confirmed by the measurement. The thermographic method is employed for this confirmation. The structural parameters are listed in Table 5.5. Figure 5.16 shows the result of measurement. Figure 5.16 (a) shows the three-dimensional SAR distribution in the observation plane and Fig. 5.16 (b) shows the two-dimensional SAR distribution on the observation line. Moreover, Fig. 5.16 (b) includes the result of calculation. From Fig. 5.16, not only the localized heating -by using the coaxial-dipole antenna- but also the validity of the result of calculation can be confirmed.

Table 5.5 Parameters for FDTD calculations.

Parameters for calculation	
Size of calculation space	$x \times y \times z$ = 54 × 54 × 160 mm
Minimum cell size	$\Delta x = \Delta y$ = 0.1 mm, Δz = 1.0 mm
Time step (for FDTD) Δt	0.235 ps (from Courant limit)
Antenna structure	
Feeding frequency	2450 MHz
$2L_d$	20.0 mm
D_t	70.0 mm
d_{bi}	0.86 mm
d_{bs}	2.19 mm
d_c	2.65 mm
ε_{rc}	2.60
ε_{ri}	2.03
Biological tissue	
Liver	ε_r = 43.03, σ = 1.69 S/m

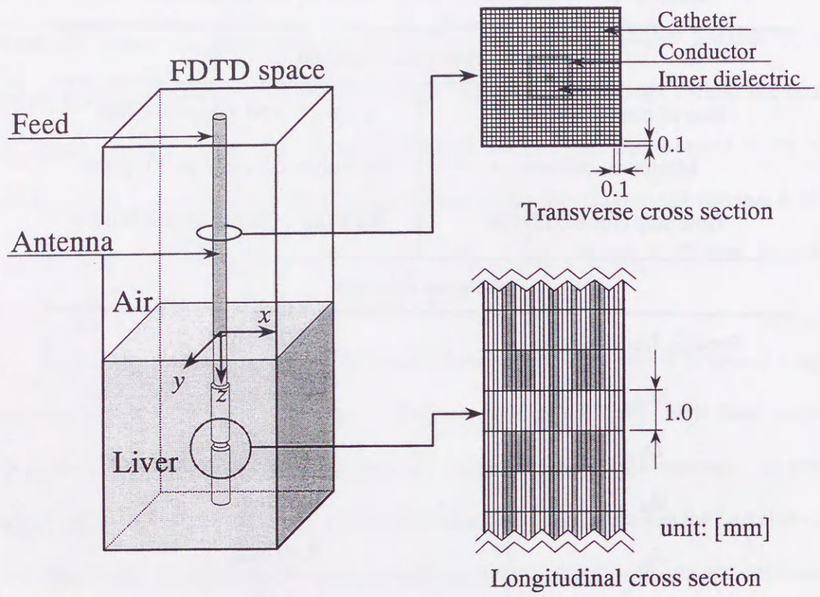

Fig. 5.14 Instance of FDTD calculation model for the coaxial-dipole antenna.

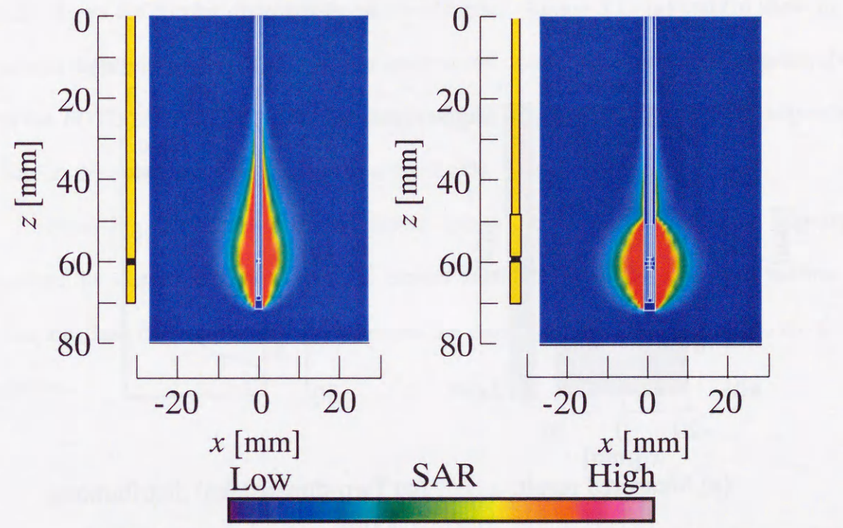

(a) Coaxial-slot antenna. (b) Coaxial-dipole antenna.

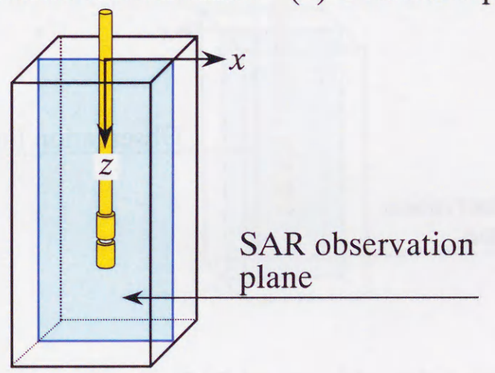

Fig. 5.15 SAR distributions around the antenna.

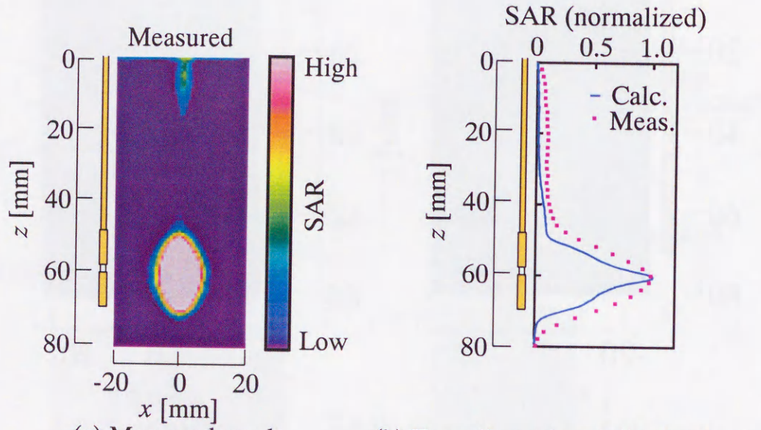

(a) Measured result. (b) Two-dimensional distributions.

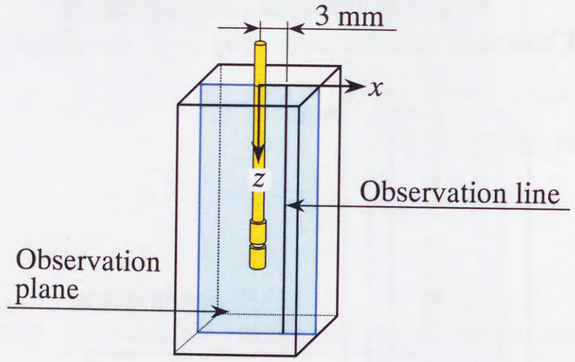

Fig. 5.16 Measured SAR distributions.

In order to understand the mechanism of generating the localized heating by the coaxial-dipole antenna, the current distribution on the antenna is calculated. Figure 5.17 shows the current distributions on the antenna. Figure 5.17 (a) and (b) show the current distributions on the coaxial-slot antenna and coaxial-dipole antenna, respectively. In the FDTD calculation, the current distribution is defined as the strength of magnetic field in the orthogonal direction to the antenna axis.

From Fig. 5.17, in the coaxial-dipole antenna, a localized distribution appears around the sleeves, compared with the current distribution on the coaxial-slot antenna. The localized current distribution generates the localized SAR distributions around the sleeves.

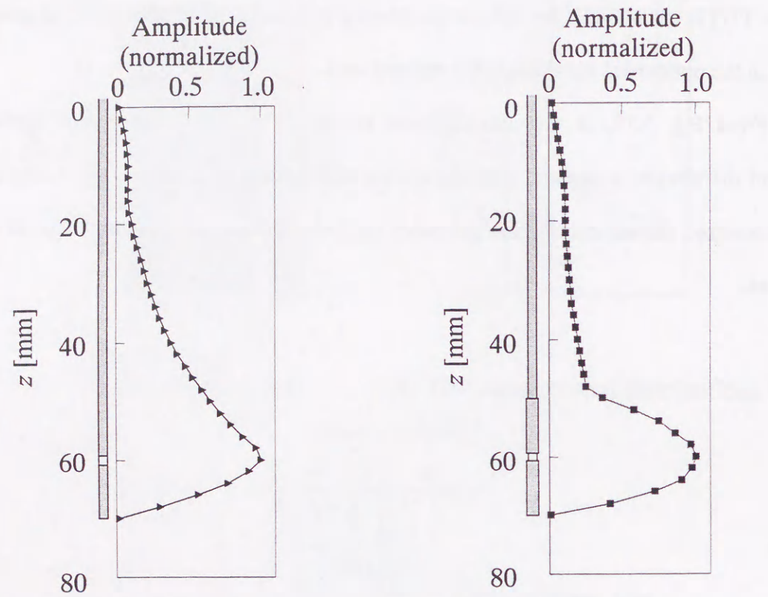

(a) Coaxial-slot antenna. (b) Coaxial-dipole antenna.

Fig. 5.17 Current distributions on the antenna.

5.5 Improvement on the coaxial-dipole antenna

5.5.1 Index for evaluating the shape of the SAR distributions

This section describes the improvement on shape of the SAR distributions around the coaxial-dipole antenna. First, in order to estimate the shape of the SAR distributions around the antenna numerically, an index is introduced. Then, the dependence of S_{11} of the antenna with the length of the sleeves is presented. By using these calculated results, the length of the sleeves is improved, not only in terms of the shape of the SAR distributions but also in terms of electrical properties of the antenna. Finally, the effectiveness of the improved antenna is confirmed by the coagulation experiment.

The index for evaluating the shape of the SAR distributions is explained in Fig. 5.18. From the clinical side, generating a spherical coagulated region at the tip of the antenna is desired. In Fig. 5.18, when the area of S_1 equals the area of S_2, the shape of the SAR distributions in the observation plane becomes a circle (it is a sphere in the three-dimension space). Therefore, the index S, defined as follows, is introduced.

$$S = \frac{S_2}{S_1} \tag{5.2}$$

When S equals 1.0, the SAR distribution becomes a circle*.

* This index S is just for the coaxial-dipole antenna, and therefore cannot be adopted for all kinds of antennas.

Figure 5.19 shows the calculated result of the dependence of the index S with the length of the sleeves. This figure includes the result of the coaxial-slot antenna for comparison. From Fig. 5.19, when the length of the sleeves is 22 mm, the index S becomes maximum and is nearly 1.0. Therefore, we may say that the coaxial-dipole antenna, whose length of the sleeves is 22 mm, has a possibility of generating a spherical coagulated region.

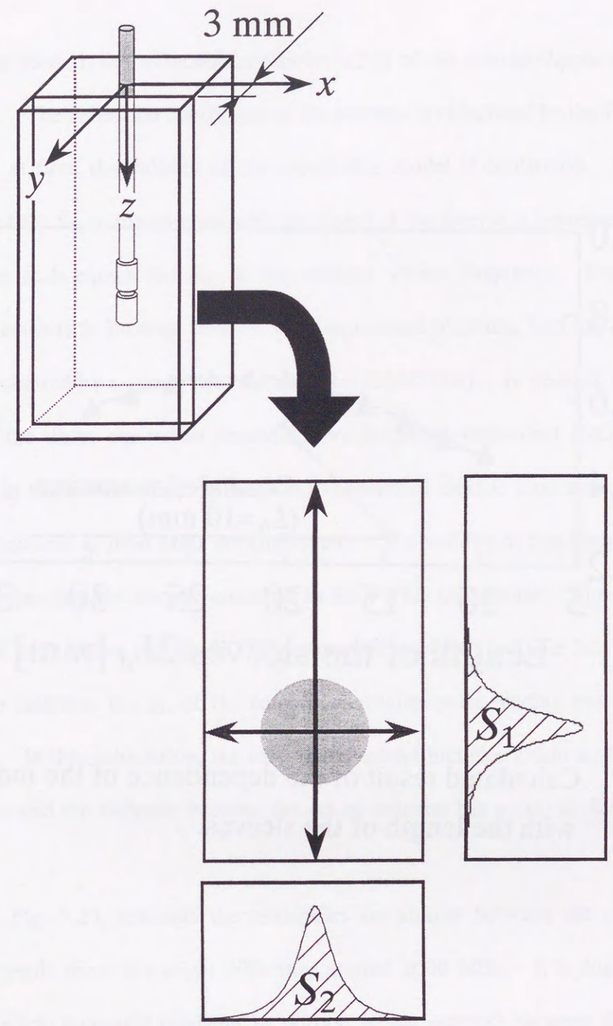

Fig. 5.18 The ideal SAR distribution.

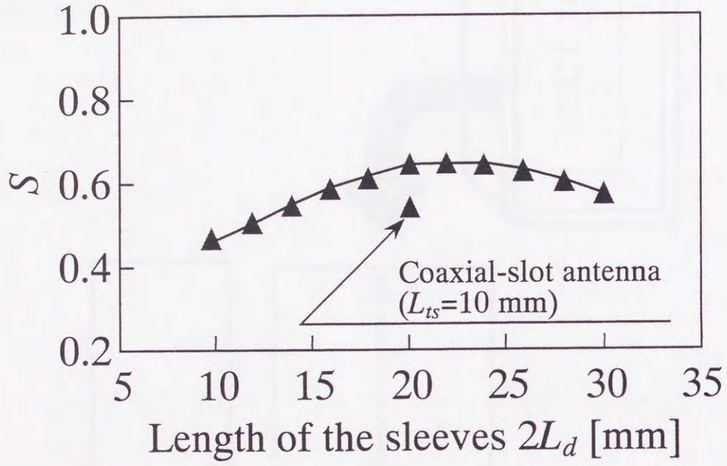

Fig. 5.19 Calculated result of the dependence of the index S with the length of the sleeves.

5.5.2 Reflection coefficient of the antenna

In this section, the reflection coefficient (S_{11}) of the coaxial-dipole antenna is investigated. The reflection coefficient of the antenna is calculated by the FDTD method. Therefore, at first, the validity of the calculation model is confirmed. Next, the dependence of the S_{11} of the antenna with the length of the sleeves is presented.

Figure 5.20 shows the S_{11} of the antenna versus frequency. Here, the coaxial-dipole antenna is inserted into the liver-equivalent phantom, and the S_{11} of the antenna is measured by a vector network analyzer (HP8753B). In general, the biological tissue and the tissue-equivalent phantom have frequency-dependent electric constants. However, in this calculation, the frequency-dependent electric constants are neglected (electric constants at 2450 MHz are employed). The validity of this hypothesis is confirmed by changing the electric constants in the FDTD calculation. The structural parameters of the antenna and the FDTD parameters are listed in Table 5.5. In addition, in order to calculate the S_{11} of the antenna, Gaussian pulse feeding and FFT [14] are employed. In this calculation, the calculation model includes a thin air layer between the antenna and the catheter, because the actual antenna has a thin air layer in this region.

From Fig. 5.20, although the tendencies are similar between the calculated and measured result, there is a slight difference around 2000 MHz. It is due to the difference of electric constants (catheter or portion of the sleeves) between the calculation model and the actual antenna.

Then, the dependence of S_{11} of the antenna with the length of the sleeves is calculated. Figure 5.21 shows the result of calculations. From Fig. 5.21, a minimum S_{11} is

observed for $2L_d$ equals to 20 mm. In this case, the coaxial-dipole antenna almost resonates around the sleeves. According to the result of the previous section, the coaxial-dipole antenna, whose length of the sleeves is 22 mm, has a possibility of generating a spherical coagulated region. Therefore, the suitable length of the sleeves is approximately 20 mm.

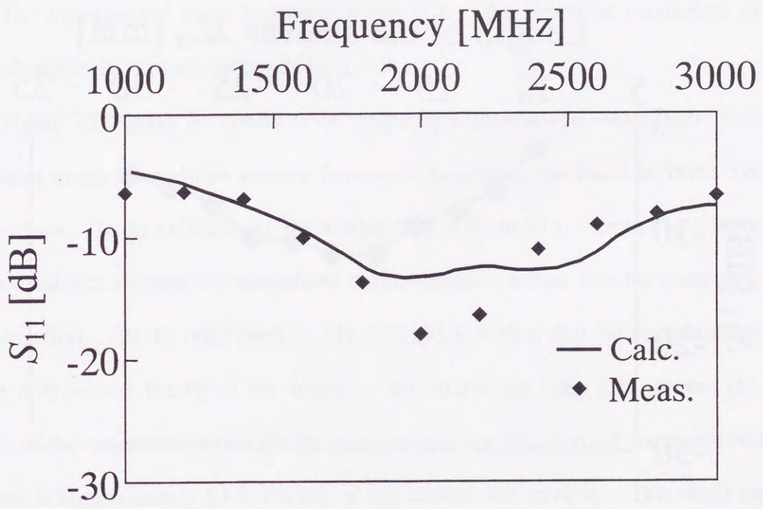

Fig. 5.20 S_{11} versus frequency of the coaxial-dipole antenna.

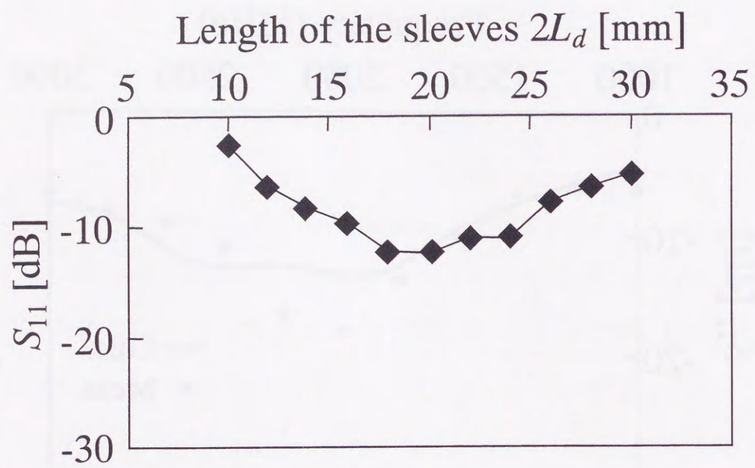

Fig. 5.21 S_{11} versus length of the sleeves $2L_d$.

5.5.3 Experimental validation

The effectiveness of the improved antenna is confirmed by conducting the coagulation experiment. From the results of Sections 5.5.1 and 5.5.2, the coaxial-dipole antenna with sleeves of $2L_d$ = 20 mm is conducted the coagulation experiment.

The experimental setup is shown in Fig. 5.7. The structural parameters of the coaxial-dipole antenna are shown in Table 5.5.

Figure 5.22 shows the results of the coagulation experiment. This figure includes the result of the coaxial-slot antenna (structural parameters are listed in Table 5.6) for comparison. In the experiments, the heating time is set to 90 s. From Fig. 5.22 (a), in the coaxial-slot antenna, the coagulated region becomes longer into the antenna insertion direction. On the other hand, in Fig. 5.22 (b), it is clear that the coagulated region exists only around the tip of the antenna. By comparing Figs. 5.22 (a) and (b), the length of the coagulated region (in the antenna insertion direction) of the coaxial-dipole antenna is approximately 50 % the one of the coaxial-slot antenna. This result means that the coaxial-dipole antenna is very useful for the localized heating.

Table 5.6 Structural parameters of the coaxial-slot antenna for comparison.

Feeding frequency	2450 MHz
L_{ts}	10.0 mm
D_t	70.0 mm
d_b	1.19 mm
d_c	2.00 mm
t_c	0.35 mm
ε_{rc}	3.50
ε_{ri}	2.03

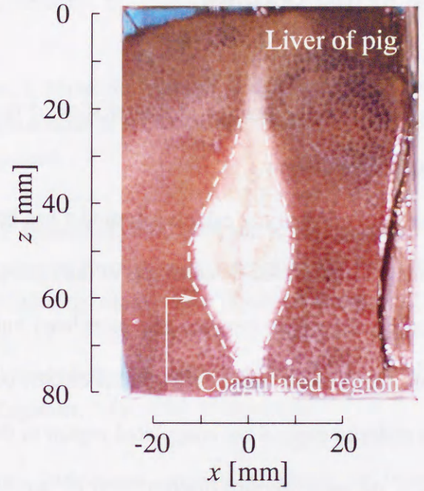

(a) Coaxial-slot antenna (net input power: 43.1 W).

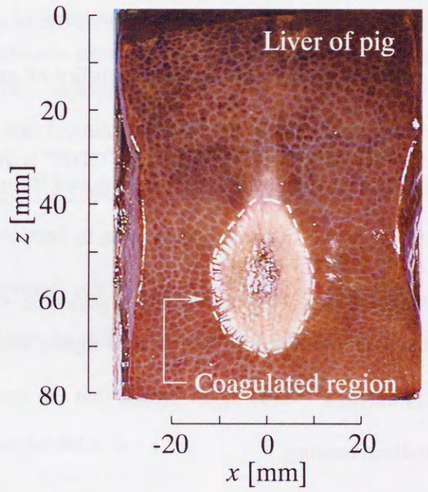

(b) Coaxial-dipole antenna (net input power: 43.6 W).

Fig. 5.22 Results of the coagulation experiment.

5.6 Conclusions in this chapter

This chapter has described the heating characteristics of the thin coaxial antenna for the microwave coagulation therapy.

In Section 5.2, the validation of the calculation model has been confirmed. Here, the temperature dependence on the electric constants of the biological tissue is included. As a result, a good agreement result between the calculated and the measured result -without considering the temperature dependence on the electric constants- is obtained.

In Section 5.3, in order to expand the coagulated region in the perpendicular direction of the antenna axis, the array applicator composed of two coaxial-slot antennas is introduced. Moreover, the heating performances of the array applicator are improved by employing the three indices for evaluating the size of the coagulated region. As a result, the two-antenna array applicator has the possibility of generating a coagulated region of 3 cm in diameter, which is desired from the clinical side.

In Section 5.4, the coaxial-dipole antenna is introduced for generating the localized heating only around the tip of the antenna. Moreover, in Section 5.5, the improvement of the coaxial-dipole antenna especially the length of the sleeves is explained. It was found that the localized heating ability of the coaxial-dipole antenna is better than the one of the coaxial-slot antenna. This result means that the coaxial-dipole antenna is very useful for the localized heating.

References in Chapter 5

[1] T. Shibata, T. Niinobu, T. Murakami, T. Ishida, N. Shibata, and M. Takami, "An experimental study on microwave coagulation in ischemic liver," Journal of Microwave Surgery, vol. 16, pp. 5-9, Nov. 1998 (in Japanese).

[2] K. Saito, S. Hosaka, Y. Hayashi, H. Yoshimura, and K. Ito, "Improvement of heating performances of thin coaxial antennas for microwave coagulation therapy," The 8th International Congress of Hyperthermic Oncology Abstract book (Kyongju, Korea), p. 127, Apr. 2000.

[3] Y. Akao, "Fundamentals of electromagnetic compatibility," Institute of Electrical, Information and Communication Engineers, Tokyo, 1991 (in Japanese).

[4] T. Seki and H. Saitsu, "*Microwave coagulation therapy for hepatocellular carcinoma*," Nankodo, Tokyo, 1999 (in Japanese).

[5] K. Saito, Y. Hayashi, H. Yoshimura, and K. Ito, "Heating characteristics of array applicator composed of two coaxial-slot antennas for microwave coagulation therapy," IEEE Transactions on Microwave Theory and Techniques, vol. 48, no. 11, pp. 1800-1806, 2000.

[6] J. Wang and O. Fujiwara, "FDTD computation of temperature rise in the human head for portable telephones," IEEE Transactions on Microwave Theory and Techniques, vol. 47, no. 8, pp. 1528-1534, 1999.

[7] K. Furuya, "The Study on heating characteristics of the coaxial-slot antenna and its evaluation method for interstitial heating," Ph. D. dissertation at Chiba University, Chiba, Japan, Jan. 1996 (in Japanese).

[8] http://www.fcc.gov/fcc-bin/dielec.sh

[9] F. A. Duck, "*Physical properties of tissue*," Academic, New York, 1990.

[10] J. Patterson and R. Strang, "The role of blood flow in hyperthermia," International Journal of Radiation Oncology Biological Physics, vol. 5, pp. 235-241, 1979.

[11] P. M. Van Den Berg, A. T. De Hoop, A. Segal, and N. Praagman, "A computational model of the electromagnetic heating of biological tissue with application to hyperthermic cancer therapy," IEEE Transactions on Biomedical Engineering, vol. BME-30, no. 12, pp. 797-805, 1983.

[12] K. Iwata, K. Udagawa, M. S. Wu, K. Ito, and H. Kasai, "A basic study of coaxial-dipole applicator for microwave interstitial hyperthermia," Proceedings of 12th Annual meeting of the Japanese Society of Hyperthermic Oncology, pp. 230-231, Sep. 1995.

[13] K. Saito, S. Hosaka, T. Taniguchi, H. Yoshimura, and K. Ito, "Improvement of heating patterns by using a coaxial-dipole antenna for microwave coagulation therapy," USNC/URSI National Radio Science Meeting 2000 Digest (Salt Lake City, USA), p. 157, Jul. 2000.

[14] T. Uno, "*Finite difference time domain method for electromagnetic field and antenna analyses*," Corona publishing, Tokyo, 1998 (in Japanese).

Chapter 6

Conclusions

This dissertation describes the heating characteristics of the thin coaxial antennas for minimally invasive microwave thermal therapy.

In recent few decades, various types of applications of the microwave have been investigated and have been applied to thermal therapy. In particular, minimally invasive interstitial therapies using thin applicators have expanded dramatically [1]. They are interstitial hyperthermia and microwave coagulation therapy for medical treatment for cancer, cardiac catheter ablation for ventricular arrhythmia treatment, and so forth. In particular, this dissertation describes the heating characteristics of the thin coaxial antenna for the interstitial microwave hyperthermia and the microwave coagulation therapy for cancer treatments.

In Chapters 2 and 3, the techniques of the peripheral for the studies such as numerical techniques and the methods of measurement were described. In addition, these techniques are employed not only for the investigation of medical regions but also for the improvement of the mobile cellular phone [2].

In Chapter 4, the heating characteristics of the coaxial-slot antenna, which is one of the thin coaxial antennas, was presented. First, the validity of the calculation model with rectangular cross section was confirmed. Second, the hot spot around the antenna insertion point was studied by using this calculation model. As a result, the SAR value

at this point is found to be approximately 85 % of the peak SAR. Third, the temperature distributions in the multilayered medium was calculated. In this case, the hot spot appeared in the fat layer. However, the on-off power feeding was found to have the possibility to reduce the hot spot in this region. Fourth, in the array applicators, the control of longitudinal heating pattern by employing the coaxial slot antennas with two slots was presented. The arbitrary shaped three-dimensional heating region will be generated by combining this technique and the technique for control of the heating pattern in perpendicular direction of the antenna axis [3]. Finally, the fundamental study for developing the treatment system combining the interstitial microwave hyperthermia and the interstitial radiation therapy was explained. This system can be realized by sharing the catheter for the interstitial microwave hyperthermia with the one for the interstitial radiation therapy. In this dissertation, the heating characteristics of the coaxial-slot antennas with the catheter for the interstitial radiation therapy were described. As the results, it was confirmed that the heating ability of the antenna with the catheter is suitable for realization of the treatment system.

In Chapter 5, the applications of thin coaxial antennas in the microwave coagulation therapy were described. There are two major problems to be improved for conventional antenna. They are "the coagulated region in the perpendicular direction of the antenna axis is insufficient" and "the shape of the coagulated region becomes longer into the antenna insertion direction". In this dissertation, the first problem has been overcome by using the array applicator composed of two coaxial-slot antennas. This result is useful for expanding the coagulated region. Therefore, there is a possibility that the region of application of the microwave coagulation therapy can be expanded. Moreover, the second problem has been improved by introducing the coaxial-dipole antenna, which is another type of the thin coaxial antenna. It was clear that the coaxial-dipole antenna generates the spherical coagulated region around the tip of the antenna. At present, there is a problem of generating the undesirable coagulated region at the blood vessel, the gallduct and so forth [4]. This problem derives from impracticability of localized heating in the conventional antenna. Therefore, introduction of the coaxial-dipole antenna improves the treatment result.

Medical applications for cancer treatment of the electromagnetic waves is still at its early age, compared to other traditional modalities such as surgical excision, chemotherapy and radiation therapy. The author will be glad if this study is of any help to the people concerning to the medical applications of the electromagnetic energy.

References in Chapter 6

[1] A. Rosen and H. D. Rosen, " RF/Microwaves in thermal therapies," Technical Report of IEICE, vol. MW98-21, pp. 59-66, May 1998.

[2] Y. Okano, "The study on the evaluation of the mutual interaction between the high-frequency near-fields and the human body," Ph. D. dissertation at Chiba University, Chiba, Japan, Jan. 1999 (in Japanese).

[3] L. Hamada, "Study on the array applicator for microwave interstitial hyperthermia," Ph. D. dissertation at Chiba University, Chiba Japan, Feb. 2000.

[4] T. Seki and H. Saitsu (Eds.), "*Microwave coagulation therapy for hepatocellular carcinoma*," Konando, Tokyo Japan, 1999 (in Japanese).

Publication list

Journals

Kazuyuki Saito and Koichi Ito, "Heating characteristics of coaxial-slot antenna for interstitial microwave hyperthermia in the multilayered media," Japanese Journal of Hyperthermic Oncology, vol. 14, no. 2, pp. 117-124, Jun. 1998 (in Japanese).

Kazuyuki Saito and Koichi Ito, "Study on SAR distribution of coaxial-slot antenna for interstitial microwave hyperthermia using FDTD method," Transactions of IEICE, vol. J82-B, no. 2, pp. 276-282, Feb. 1999 (in Japanese).

Kazuyuki Saito, Osamu Nakayama, Lira Hamada, and Koichi Ito, "Analysis of temperature distributions generated by square array applicator composed of coaxial-slot antenna for hyperthermia," Transactions of IEICE, vol. J82-B, no. 9, pp. 1730-1738, Sep. 1999 (in Japanese).

Kazuyuki Saito, Yoshihiko Hayashi, Hiroyuki Yoshimura, and Koichi Ito, "Heating characteristics of array applicator composed of two coaxial-slot antennas for microwave coagulation therapy," IEEE Transactions on Microwave Theory and Techniques, vol. 48, no. 11, pp. 1800-1806, Nov. 2000.

Other papers

Kazuyuki Saito, Lira Hamada, Koichi Ito, and Hiroyuki Kamei, "A basic study on the measurement of the permittivity of the soil by using the coaxial dipole antenna," Journal of the institute of image information and television engineers, vol. 52, no. 8, pp. 1239-1242, Aug. 1998 (in Japanese).

Lira Hamada, Kazuyuki Saito, Hiroyuki Yoshimura, and Koichi Ito, "Dielectric-loaded coaxial-slot antenna for interstitial microwave hyperthermia: longitudinal control of heating patterns," International Journal of Hyperthermia, vol. 16, no. 3, pp. 219-229, Mar. 2000.

Hideo Saotome, Kazuyuki Saito, Mieko Ueda, and Yo Sakaki, "Linear actuator with flat-ring-shaped magnets," The Transactions of The Institute of Electrical Engineers of Japan, vol. 117-A, no. 2, pp. 118-121, Feb. 2000.

Writing

Koichi Ito, Hiroyuki Yoshimura, Kazuyuki Saito, and Lira Hamada, "Current trend of antennas for medical application," Electronics, Ohm-sha, Tokyo, vol. 44, no. 2, pp. 68-72 (in Japanese).

Awards

1997 IEICE AP-S Freshman Award (December 18, 1997)

1999 URSI General Assembly Award (August 13, 1999)

2000 IEEE AP-S Japan Chapter Young Engineer Award (December 14, 2000)

International conferences

Kazuyuki Saito, Lira Hamada, and Koichi Ito, "A practical study of coaxial-slot antenna for interstitial microwave hyperthermia," Proceedings of the 1997 Thailand-Japan Joint Symposium on Antennas and Propagation (Bangkok, Thailand), vol. AP97-29, pp. 49-54, May 1997.

Kazuyuki Saito, Osamu Nakayama, Lira Hamada, Hiroyuki Yoshimura, and Koichi Ito, "Basic study of the coaxial-slot antennas for minimally invasive microwave thermal therapy," Proceedings of the 20th Annual International Conference of the IEEE Engineering in Medicine and Biology Society (Hong Kong, China), vol. 20, no. 6, pp. 3261-3264, Oct. 1998.

Kazuyuki Saito, Osamu Nakayama, Lira Hamada, Hiroyuki Yoshimura, and Koichi Ito, "FDTD analysis on the coaxial antennas for minimally invasive microwave thermal therapy," Proceedings of 1998 Asia-Pacific Microwave Conference (Yokohama, Japan), vol. 2, pp. 881-884, Dec. 1998.

Kazuyuki Saito, Yoshihiko Hayashi, Hiroyuki Yoshimura, and Koichi Ito, "Application of thin coaxial antenna to microwave coagulation therapy: a basic study," Proceedings of Progress in Electromagnetics Research Symposium (Taipei, Taiwan), vol. 1, p. 436, Mar. 1999.

Kazuyuki Saito, Yoshihiko Hayashi, Hiroyuki Yoshimura, and Koichi Ito, "Numerical analysis of thin coaxial antennas for microwave coagulation therapy," Digest of IEEE Antennas and Propagation Society International Symposium (Orlando, USA), vol. 2, pp. 992-995, Jul. 1999.

Kazuyuki Saito, Yoshihiko Hayashi, Hiroyuki Yoshimura, and Koichi Ito, "Analysis of thermal distributions produced by thin coaxial antenna for microwave coagulation therapy," Abstracts of 26th International Union of Radio Science General Assembly (Toronto, Canada), p. 641, Aug. 1999.

Kazuyuki Saito, Sumie Hosaka, Yoshihiko Hayashi, Hiroyuki Yoshimura, and Koichi Ito, "Improvement of heating characteristics of thin coaxial-antennas for microwave coagulation therapy," Abstract book of the 8th International Congress of Hyperthermic Oncology 2000 (Kyongju, Korea), p. 127, p. 258, Apr. 2000.

Kazuyuki Saito, Sumie Hosaka, Takeshi Taniguchi, Hiroyuki Yoshimura, and Koichi Ito, "Improvement of heating patterns by using a coaxial-dipole antenna for microwave coagulation therapy," Digest of International Union of Radio Science Meeting (Salt Lake City, USA), p. 157, Jul. 2000.

Kazuyuki Saito, Sumie Hosaka, Yoshihiko Hayashi, Hiroyuki Yoshimura, and Koichi Ito, "Localized heating by the coaxial-dipole antenna for microwave coagulation therapy," Proceedings of 5th International Symposium on Antennas, Propagation, and EM Theory (Beijing, China), pp. 406-409, Aug. 2000.

Kazuyuki Saito, Sumie Hosaka, Yoshihiko Hayashi, Hiroyuki Yoshimura, and Koichi Ito, "Heating patterns of coaxial-dipole antennas for microwave coagulation therapy," Proceedings of the 2000 International Symposium on Antennas and Propagation (Fukuoka, Japan), vol. 1, pp. 237-240, Aug. 2000.

Koichi Ito, Hiroyuki Yoshimura, Kazuyuki Saito, and Lira Hamada, "Heating characteristics of coaxial-slot antenna for minimally invasive thermal therapy," Proceedings of SPIE Conference on Thermal Treatment of Tissue with Image Guidance (San Jose, USA), vol. 3594, pp. 68-79, Jan 1999.

Koichi Ito, Kazuyuki Saito, and Hiroyuki Yoshimura, "Microwave antennas for thermal therapy applications," Proceedings of 7th International Symposium on Recent Advances in Microwave Technology (Málaga, Spain), pp. 574-577, Dec. 1999.

Koichi Ito, Kazuyuki Saito, and Hiroyuki Yoshimura, "Improvement of antennas for minimally invasive microwave thermal therapy," World Congress on Medical Physics and Biomedical Engineering (Chicago, USA), Medical Physics, vol. 27, no. 6, p. 1408, Jul. 2000.

Takeshi Taniguchi, Kazuyuki Saito, Sumie Hosaka, Hiroyuki Yoshimura, and Koichi Ito, "Localized heating and expansion of heating region by using thin coaxial antennas for microwave coagulation therapy," Proceedings of 2000 Asia-Pacific Symposium on Broadcasting and Communications (Bangkok, Thailand), pp. 134-139, Dec. 2000.

Acknowledgements

I would like to thank the continuing guidance and encouragement of Professor Koichi Ito. It has a great honor and at the same time a great experience to study under his instruction.

I would also like to thank Professor Hiroyuki Yoshimura for his valuable guidance and many helpful discussions. Thanks are also due to Dr. Hiroko O. Ueda for her helpful comments. The author is indebted to Professor Nobuo Takeuchi, Professor Hiroyuki Hachiya, and Professor Toshiaki Takano for their helpful discussion on this dissertation.

I also express my appreciation to Mr. Ichirou Ida, Mr. Takefumi Namiki and Mr. Yoshio Koyanagi for their frequent, stimulating and helpful comments.

I wish to express my sincere gratitude to Dr. Lira Hamada, Dr. Katsumi Furuya, and Dr. Yoshinobu Okano, who are the excellent graduates of Chiba University, for their useful comments.

I would like to thank the Japanese Society of Hyperthermic Oncology and Technical Groups of IEICE: Antenna and Propagation Group and Human Phantoms for Electromagnetics Group for helpful comments, and AZWELL Inc. for providing the microwave generator. I also would like to thank Professor Shizuo Mizushina from Shizuoka University, Professor Yoji Kotsuka from Tokai University, Professor Hirokazu Kato from Okayama University, Dr. Takehide Asano from the Faculty of Medicine at Chiba University, Professor Yutaka Aoyagi from Tokyo Dental College, Ichikawa General Hospital, Dr. Iwao Tsukiyama from Tochigi Prefectural Cancer Center Hospital, Pro-

fessor Masahiro Hiraoka form Kyoto University, Professor Paul R. Stauffer from University of California at San Francisco, Professor James C. Lin from University of Illinois at Chicago, and Dr. C. K. Chou from Motorola Inc. for their helpful comments.

This study was supported in part by the Japan Society for the Promotion of Science, and I would like to highlight here the generosity of this organization.

I would like to thank to all the students who assisted me by taking the time to complete this dissertation.

I wish to acknowledge all the other people who have contributed to the completion of this dissertation.

At last, I express the respects to my parents for their financial and mental support.

Appendix 1

Finite difference time domain (FDTD) method

The finite difference time domain (FDTD) method is one of the numerical techniques, which solves the Maxwell's equations of differential form in the time domain. The FDTD method was proposed by Yee [1]. At present, the FDTD method is widely employed for solving the electromagnetic problems such as improvement of structure of the antenna, research on the interaction between the electromagnetic fields and the human body, and so on.

The finite difference approximation of the FDTD method is written as follows:

$$
\begin{aligned}
E_x^n\left(i+\frac{1}{2},j,k\right) = {} & \frac{\varepsilon\left(i+\frac{1}{2},j,k\right)}{\varepsilon\left(i+\frac{1}{2},j,k\right)+\sigma\left(i+\frac{1}{2},j,k\right)\Delta t} E_x^{n-1}\left(i+\frac{1}{2},j,k\right) \\
& + \frac{\Delta t}{\varepsilon\left(i+\frac{1}{2},j,k\right)+\sigma\left(i+\frac{1}{2},j,k\right)\Delta t} \\
& \times \left[\begin{array}{l} \dfrac{1}{\Delta y}\left\{H_z^{n-\frac{1}{2}}\left(i+\frac{1}{2},j+\frac{1}{2},k\right)-H_z^{n-\frac{1}{2}}\left(i+\frac{1}{2},j-\frac{1}{2},k\right)\right\} \\ -\dfrac{1}{\Delta z}\left\{H_y^{n-\frac{1}{2}}\left(i+\frac{1}{2},j,k+\frac{1}{2}\right)-H_y^{n-\frac{1}{2}}\left(i+\frac{1}{2},j,k-\frac{1}{2}\right)\right\} \end{array}\right].
\end{aligned}
\tag{A1.1}
$$

$$H_x^{n+\frac{1}{2}}\left(i,j+\frac{1}{2},k+\frac{1}{2}\right)=H_x^{n-\frac{1}{2}}\left(i,j+\frac{1}{2},k+\frac{1}{2}\right)+\frac{\Delta t}{\mu\left(i,j+\frac{1}{2},k+\frac{1}{2}\right)}\times\left[\begin{array}{l}\frac{1}{\Delta y}\left\{E_z^n\left(i,j+1,k+\frac{1}{2}\right)-E_z^n\left(i,j,k+\frac{1}{2}\right)\right\}\\-\frac{1}{\Delta z}\left\{E_y^n\left(i,j+\frac{1}{2},k+1\right)-E_y^n\left(i,j+\frac{1}{2},k\right)\right\}\end{array}\right]. \quad \text{(A1.2)}$$

Here, for a continuous function of space and time $f(x,y,z,t)$, its discretized form at nth time step can be written as $f^n{}_{ijk}=f(i\Delta x, j\Delta y, k\Delta z, n\Delta t)$, where Δx, Δy and Δz are cell sizes in the finite difference representation and Δt is the incremental time step. Other components E_y, E_z, H_y,and H_z are given by the same [2].

Appendix 2

Finite difference approximation of bioheat transfer equation

The result of calculation by using the following finite difference approximation is the temperature rise from the initial temperature and it was assumed that T_b (temperature of the blood) was equal to the initial temperature.

The finite difference approximation of the bioheat transfer equation can be written as follows:

$$T_{ijk}^{n+1}=\frac{\kappa_{ijk}\,\Delta t}{\rho_{ijk}\,c_{ijk}}\left(C1x_{ijk}T_{i-1jk}^n+C3x_{ijk}T_{i+1jk}^n+C1y_{ijk}T_{ij-1k}^n+C3y_{ijk}T_{ij+1k}^n+C1z_{ijk}T_{ijk-1}^n+C3z_{ijk}T_{ijk+1}^n\right)+\left\{1-\left(C2x_{ijk}+C2y_{ijk}+C2z_{ijk}\right)\frac{\kappa_{ijk}\,\Delta t}{\rho_{ijk}\,c_{ijk}}-\frac{\rho_{ijk}\,\rho_{bijk}\,c_{bijk}\,F_{ijk}\,\Delta t}{\rho_{ijk}\,c_{ijk}}\right\}T_{ijk}^n+\frac{\Delta t}{c_{ijk}}\mathrm{SAR}_{ijk} \quad \text{(A2.1)}$$

$$C1x_{ijk}=\frac{8}{\left(\Delta x_{i-1jk}+\Delta x_{ijk}\right)\left(\Delta x_{i-1jk}+2\Delta x_{ijk}+\Delta x_{i+1jk}\right)} \quad \text{(A2.2)}$$

$$C2x_{ijk}=\frac{8}{\left(\Delta x_{i-1jk}+\Delta x_{ijk}\right)\left(\Delta x_{ijk}+\Delta x_{i+1jk}\right)} \quad \text{(A2.3)}$$

$$C3x_{ijk}=\frac{8}{\left(\Delta x_{ijk}+\Delta x_{i+1jk}\right)\left(\Delta x_{i-1jk}+2\Delta x_{ijk}+\Delta x_{i+1jk}\right)}. \quad \text{(A2.4)}$$

Here, for a continuous function of space and time $f(x,y,z,t)$, its discretized form at nth time step can be written as $f^n{}_{ijk}=f(i\Delta x, j\Delta y, k\Delta z, n\Delta t)$, where Δx, Δy and Δz are cell sizes in the finite difference representation and Δt is the incremental time step. Other coefficients $C1y_{ijk}$, $C2y_{ijk}$, $C3y_{ijk}$, $C1z_{ijk}$, $C2z_{ijk}$ and $C3z_{ijk}$ in Eq. (A2.1) are given by replacing x in Eqs. (A2.2), (A2.3) and (A2.4) by y and z.

References in Appendix

[1] K. S. Yee, "Numerical solution of initial boundary value problems involving Maxwell's equations in isotropic media," IEEE Transactions on Antennas and Propagations, vol. AP-14, no. 3, pp. 302-307, 1966.

[2] T. Uno, "*Finite difference time domain method for electromagnetic field and antenna analyses*," Corona publishing, Tokyo, 1998 (in Japanese).